

1 **Gliding through marine heatwaves: Subsurface biogeochemical**
2 **characteristics on the Australian continental shelf**

3

4 Daneeja Mawren^{1,2,3*}, Julia Araujo⁴, Romain Le Gendre⁵, Jessica A. Benthuisen⁶, Franck Eitel
5 Kemgang Ghomsi^{1,7,8}, Jayanthi S. Saranya⁹, Amandine Schaeffer^{10,11}

6

7 ¹Department of Oceanography, University of Cape Town, Cape Town, South Africa

8 ²South African Environmental Observation Network, Egagasini Node, Roggebaai, South Africa

9 ³Mascarene Environmental Consulting, Ltd, Mauritius

10 ⁴National Center for Monitoring and Early Warning of Natural Disasters (CEMADEN), São José dos
11 Campos,12630-000, Brazil

12 ⁵IFREMER, UMR 9220 ENTROPIE (IRD, Reunion Univ., IFREMER, New Caledonia Univ., CNRS), BP 32078,
13 98897 Noumea Cedex, New Caledonia

14 ⁶Australian Institute of Marine Science, Crawley, Western Australia 6009, Australia

15 ⁷Geodesy Research Laboratory, National Institute of Cartography, P.O. Box 157, Yaoundé, Cameroon

16 ⁸Centre for Earth Observation Science, University of Manitoba, Winnipeg, MB, Canada

17 ⁹School of Earth and Environmental Sciences, College of Natural Sciences, Seoul National University, Seoul,
18 Republic of Korea

19 ¹⁰School of Mathematics and Statistics, University of New South Wales, Sydney, New South Wales, Australia

20 ¹¹Centre for Marine Science and Innovation, University of New South Wales, Sydney, New South Wales, Australia

21

22 * *Correspondence to:* Daneeja Mawren (daneejamawren@gmail.com)

23

24

25

26 **Abstract**

27 Marine heatwaves (MHWs) disrupt ecosystems across multiple trophic levels by altering oxygen and biological
28 productivity through the water column and yet, most studies focus on the surface, overlooking subsurface processes
29 that shape ecosystem responses. To address this gap, we analysed 16 years of routine and event-based glider
30 observations on the continental shelf around Australia to present the first comprehensive assessment of the
31 subsurface biogeochemical response during surface MHWs across four contrasting coastal regions.

32 Across all regions and seasons, the distribution of chlorophyll concentrations shifted towards a decline in the mixed
33 layer and an increase below the mixed layer during MHWs, modulated by the event categories. Dissolved oxygen
34 shows a more complex distribution, which also varies during moderate and strong MHW events, arguably with more
35 variation in the mixed layer than below.

36 When regional and seasonal specificities are taken into account, the subsurface characteristics of MHWs vary in
37 accordance with the environmental setting, including the continental shelf structures, tropical / sub-tropical regimes,
38 and boundary current influences, especially through the changes in stratification. Summer surface MHWs were
39 characterised by a shallower mixed layer depth than normal conditions and enhanced stratification, confining
40 warming to the upper ocean, while other seasons allow deeper penetration under weakly stratified conditions. With
41 the shoaling of the mixed layer, enhanced stratification retained nutrients within the euphotic zone, allowing
42 phytoplankton to form deeper and intensified chlorophyll maxima. The depth of maximum stratification therefore
43 emerged as a useful proxy for the vertical extent of MHWs.

44 The interaction between physical processes, such as seasonal circulation and stratification, and biological feedback,
45 including the presence of deep chlorophyll maxima and potential oxygen production, highlights the complex
46 biogeochemical responses to MHWs, and underscores the importance of region-specific dynamics and the need for
47 more consistent observation strategy, including biogeochemical processes.

48

49 **Keywords**

50 Marine heatwaves; subsurface layers; stratification; biogeochemistry; chlorophyll; dissolved oxygen; glider
51 observations; in situ measurements; coastal waters; continental shelf; Australia.

52

53 **Short summary**

54 Using sixteen years of ocean glider observations, we show that marine heatwaves are characterised by shallower
55 mixed layers and can alter subsurface biogeochemistry across Australia's continental shelf. While surface
56 chlorophyll generally declined, strong stratification and event severity promoted deeper, intensified chlorophyll
57 maxima while subsurface oxygen responses varied. These findings underscore the importance of region-specific
58 dynamics in shaping ecological responses to marine heatwaves.

59

60 1. Introduction

61 As the Earth's climate continues to warm, the frequency and intensity of extreme events are increasing due to
62 anthropogenic forcing (Frölicher et al., 2018; Laufkötter et al., 2020) with profound consequences for both
63 ecosystems and human societies (Smith et al., 2021; 2023). Marine heatwaves (MHWs) are defined as extremely
64 warm ocean temperature anomalies and have become an increasing focus of research for their important impacts on
65 ecosystems. A key factor controlling MHW characteristics, including their vertical extent, intensity and persistence,
66 is upper-ocean stratification (Schaeffer and Roughan, 2017; Schaeffer et al., 2023; Zhang et al., 2023). Global
67 stratification has intensified over recent decades, leading to widespread mixed layer shoaling and altered
68 thermocline structure (Alexander et al., 2019; Li et al., 2020; Kwiatkowski et al., 2020; Amaya et al., 2021; Zhang et
69 al., 2023). At regional and coastal scales, stratification is further shaped by local thermal, salinity and mechanical
70 processes that regulate the vertical mixing and influence the occurrence of MHWs (Fordyce et al., 2019; Amaya et
71 al., 2021; Gao et al., 2020; Schaeffer et al., 2023). Recent studies have shown that subsurface signatures of MHWs
72 can differ substantially from surface observations. For instance, during the 2019 North Pacific MHW (“The Blob”),
73 subsurface warming persisted long after surface temperatures returned to normal, leading to prolonged ecological
74 stress at depth (Amaya et al., 2020). Similarly, along the east coast of Australia in New South Wales, subsurface
75 MHWs have been documented with minimal surface expression, highlighting the need for vertical profiling,
76 particularly in coastal regions where strong stratification, complex circulation and shallow bathymetry can amplify
77 subsurface temperature anomalies (Schaeffer and Roughan, 2017; Schaeffer et al., 2023). Strong stratification can
78 trap heat near the surface or isolate warm anomalies below the mixed layer, allowing subsurface MHWs to persist at
79 depth.

80

81 Investigating subsurface dynamics of MHWs in coastal areas is therefore critical for assessing ecological and
82 socio-economic impacts. In coastal regions and over continental shelves, subsurface biogeochemical processes play
83 a central role in sustaining vital ecosystem services such as biodiversity, carbon sequestration and nutrient cycling,
84 while supporting economic activities such as fisheries and aquaculture (Walsh, 1991; Siefert and Plattner, 2004;
85 Marre et al., 2015). When combined with MHWs, biogeochemical extremes can trigger severe ecological disruption,
86 amplifying existing environmental stressors, such as nutrient limitation (Cavole et al., 2016; Le Grix et al., 2020),
87 acidification, and deoxygenation (Tassone et al., 2022), ultimately reducing productivity and threatening marine
88 ecosystem health.

89

90 Understanding how MHWs influence key biogeochemical variables, such as chlorophyll-a concentrations and
91 oxygen levels, is essential for predicting ecosystem responses. For instance, nutrient scarcity during MHWs can
92 limit phytoplankton growth, while warmer waters increase metabolic demands in marine species, further straining
93 ecosystems (Chen et al., 2023). Although surface chlorophyll-a often decreases during MHWs (Le Grix et al., 2020),
94 responses vary depending on factors such as light and nutrient availability (Sen Gupta et al., 2020; Noh et al., 2022).

95 In regions where stratification limits nutrient upwelling, phytoplankton productivity may decrease, whereas, at
96 higher latitudes (where light is a limiting factor), stratification can enhance productivity by maintaining
97 phytoplankton in the sunlit surface layers (Kwiatkowski et al., 2020). On a global scale, MHWs have been found to
98 promote the development of deep chlorophyll maxima, based on 17 years of biogeochemical-Argo float data (Ma
99 and Chen, 2025). Reduced dissolved oxygen during MHWs represents another critical issue, particularly in shallow
100 coastal areas. Warmer water temperatures decrease oxygen solubility, potentially leading to hypoxic conditions that
101 can severely affect marine life (Meier et al., 2018; Safonova et al., 2024). MHWs intensify this mismatch between
102 oxygen supply and demand, as respiration rates increase in response to higher temperatures, further depleting
103 oxygen levels (Tassone et al., 2022). Combined effect of MHWs, reduced oxygen levels, and habitat compression
104 can trigger mass mortality events across multiple taxa, including fish, seagrasses, and marine mammals (Sampaio et
105 al., 2021; Holbrook et al., 2022), while altered prey distribution and increased metabolic demands can produce
106 cascading effects throughout marine food webs (Smith et al., 2023; Gomes et al., 2024).

107

108 While long-term satellite-derived records of sea surface temperature (SST) and surface chlorophyll-a have advanced
109 our understanding of MHWs globally, they require concurrent in water measurements to assess the extent of
110 subsurface temperature extremes and biogeochemical changes given the range of ecological impacts that can occur
111 through the water column (Smith et al., 2023). Traditional in situ methods such as moored temperature
112 measurements, conductivity-temperature-depth, and expendable bathythermograph casts can provide vertical
113 profiles, but these observations are often limited in spatial and temporal coverage (Oliver et al., 2021; Malan et al.,
114 2025; Le Gendre et al., 2025) and rarely include biogeochemical observations. In addition, coastal numerical models
115 offer valuable simulations of subsurface thermal structures, but they require large amounts of high-resolution data
116 for validation or assimilation, as they remain prone to uncertainties in poorly observed regions (Lachkar et al.,
117 2019).

118

119 Ocean gliders offer a major advancement in subsurface monitoring, through high-resolution, autonomous, and
120 continuous measurements of water temperature, salinity, and biogeochemical properties, including dissolved oxygen
121 and chlorophyll fluorescence (Testor et al., 2019). Although glider deployments have limited temporal coverage for
122 detecting extremes, their ability to sample across depths and regions provides an unprecedented view in shelf and
123 boundary current environments (Testor et al., 2019). These measurements can be used to infer stratification and
124 phytoplankton dynamics. Furthermore, event-based approaches, where gliders are deployed specifically to sample
125 MHWs, can provide real-time, dynamic insights into the subsurface evolution and intensity of these events,
126 delivering essential input to immediate ecosystem response strategies (Davies et al., 2021; Benthuisen et al., 2025).
127 Previous studies have made notable strides on better understanding the subsurface dynamics and biogeochemical
128 variability using gliders off the Australian coast (Pattiaratchi et al., 2011; Schaeffer et al., 2016a,b; Chen et al., 2019;
129 Chen et al., 2020; Ridgway and Ling, 2023). However, most of these works focused on specific regions off the
130 Australian coast or were limited to specific events, typically ranging from weeks to months, rather than continual

131 monitoring. While these studies did not explicitly focus on MHWs, gliders have been demonstrated as a useful
132 platform to capture the vertical extent of extreme warming, such as during the 2016 austral summer MHW off
133 northeastern Australia (Benthuisen et al., 2018), highlighting the role of glider observations to inform MHW
134 studies.

135

136 To address this gap, our study leverages data from the Australian Integrated Marine Observing System (IMOS)
137 gliders which provide high-resolution subsurface observations along the Australian continental shelf since 2007
138 (Pattiaratchi et al., 2017). By combining these repeated glider measurements with satellite-derived surface data, we
139 aim to provide a seasonal and regional comparison across four distinct Australian shelf regions, highlighting broader
140 patterns of subsurface MHW characteristics and their impacts on key biogeochemical variables. Specifically, we test
141 the following hypotheses: (1) surface MHWs can lead to reduced chlorophyll concentrations and lower dissolved
142 oxygen levels at the surface; (2) despite surface reductions, MHWs may promote deeper chlorophyll maxima and
143 higher dissolved oxygen concentrations at depth, potentially via enhanced subsurface productivity; (3) the depth
144 extent of surface MHWs varies with regions and seasons, and therefore establishing seasonal and regional baselines
145 are important to interpret anomalies; and (4) the severity of MHW-induced stratification modulates biogeochemical
146 variables (dissolved oxygen and chlorophyll).

147

148 The following sections outline our approach and findings: Sect. 2 describes the SST and glider datasets, statistical
149 methods, and MHWs metrics. Sect. 3.1 describes the characteristics of surface MHWs in the study regions.
150 Hypotheses (1) and (2) are examined in Sect. 3.2, which investigates how MHW severity influences chlorophyll and
151 dissolved oxygen within and below the surface mixed layer. Hypothesis (3) is addressed in Sect. 3.3, where we
152 explore regional and seasonal variations in the depth extent of MHWs, stratification and associated biogeochemical
153 profiles. Hypothesis (4) is evaluated across Sects. 3.2 and 3.3, which together assess how MHWs modulates
154 subsurface biogeochemical signatures in different regimes, based on their stratification, chlorophyll and oxygen
155 regimes. Finally, Sect. 4 discusses these findings in the context of previous global and Australian studies, leading to
156 the Conclusions in Sect. 5.

157

158

159 **2. Data and Methods**

160 **2.1 Satellite dataset and surface MHW detection**

161 Given the coastal scale of our study, we used the National Oceanic and Atmospheric Administration (NOAA)
162 CoralTemp v3.1¹ Sea Surface Temperature (SST) product, which integrates three L4 satellite SST analysis products,
163 to provide a global, daily, gap-free gridded, night-time SST field at 0.05° horizontal resolution since 1985 (Skirving

¹ CoralTemp v3.1 product's website: <https://coralreefwatch.noaa.gov/product/5km/index.php>.

164 et al., 2020). This dataset is used to track surface MHWs in near real-time² using the definition and criteria of
165 Hobday et al., (2016), which detects temperature events exceeding a locally determined upper threshold of the 90th
166 percentile relative to the long-term day-of-the-year climatology for a minimum of five consecutive days, with no gap
167 of more than two days. The baseline climatological period was defined here as a 30-year period between 1985 and
168 2014, following recommendations of Hobday et al. (2016). The MHW detection and analysis were performed using
169 the Python module available at <https://github.com/ecjoliver/marineHeatWaves>. We extracted the SST dataset over
170 the period from 1 January 1985 to 30 June 2025 and the following MHW metrics were analysed over our study
171 period from 2009 to mid-2025: the total number of events, the mean duration of the MHW events, and the mean
172 severity of the MHW (Eq. 1; following Sen Gupta et al., 2020).

173

174 2.2 Glider dataset

175 To assess the subsurface structure of MHWs, our study benefited from the Australian national glider data acquisition
176 strategy set up in 2007 by the Ocean Gliders facility under IMOS (Pattiaratchi et al., 2017). Subsequently, IMOS
177 enabled the routine deployment of gliders on the continental shelves around Australia for sustainable observations.
178 This facility has been augmented by event-based sampling of MHWs since December 2018 (Benthuisen et al.,
179 2025), delivering subsurface measurements of oceanographic parameters along with other near-real time platforms
180 during events (e.g. Box 2 of Capotondi et al., 2024). Ocean gliders are autonomous vehicles which alter their
181 buoyancy to travel up and down the water column while sampling seawater properties (Rudnick, 2016). We used
182 data from IMOS using Teledyne Webb Research Slocum Electric Gliders (G1, G2 and G3), equipped with
183 Seabird-CTD, WETLabs BBFL2SLO 3 Eco Puck sensor measuring chlorophyll fluorescence, colored dissolved
184 organic matter (CDOM) and 660 nm backscatter, and an Aanderaa Oxygen optode (Pattiaratchi et al., 2011; Chen et
185 al., 2020). Missions typically last between three to five weeks, with a maximum depth of 200 m. For this study, we
186 focus on measurements of ocean temperature, salinity, chlorophyll-a fluorescence (proxy for phytoplankton
187 concentration; Blondeau-Patissier et al., 2014), and dissolved oxygen. The measurements undertake a delayed-mode
188 quality control (Woo and Gourcuff, 2023) and are made publicly available through IMOS on the Australian Ocean
189 Data Network (AODN) Portal³.

190

191 2.3 Study regions

192 The analysis of all available deployments led us to the definition of four main regions of interest encompassing the
193 highest density of gliders transects between 2009 and 2025: (i) northeastern Australia off Queensland (QLD),
194 confined within the limits of 144.7° E to 148.0° E and 13.3° S to 19.7° S; (ii) southeastern Australia off New South
195 Wales (NSW), from 149.7° E to 154.7° E and 28.5° S to 36.7° S; (iii) southwest Western Australia (SW WA), from
196 113.2° E to 116.1° E and 29.1° S to 33.5° S; and (iv) the eastern coast of Tasmania (TAS), from 146.8° E to 149.5° E

² NOAA Coral Reef Watch marine heatwave website: https://coralreefwatch.noaa.gov/product/marine_heatwave/.

³ Australian Ocean Data Network (AODN) website: <https://portal.aodn.org.au/>.

197 and 40.5° S to 44.6° S (Fig. 1). These regions encompass contrasting continental shelf systems influenced by distinct 198 physical processes, enabling us to assess how MHWs impact biogeochemical conditions under different dynamics.

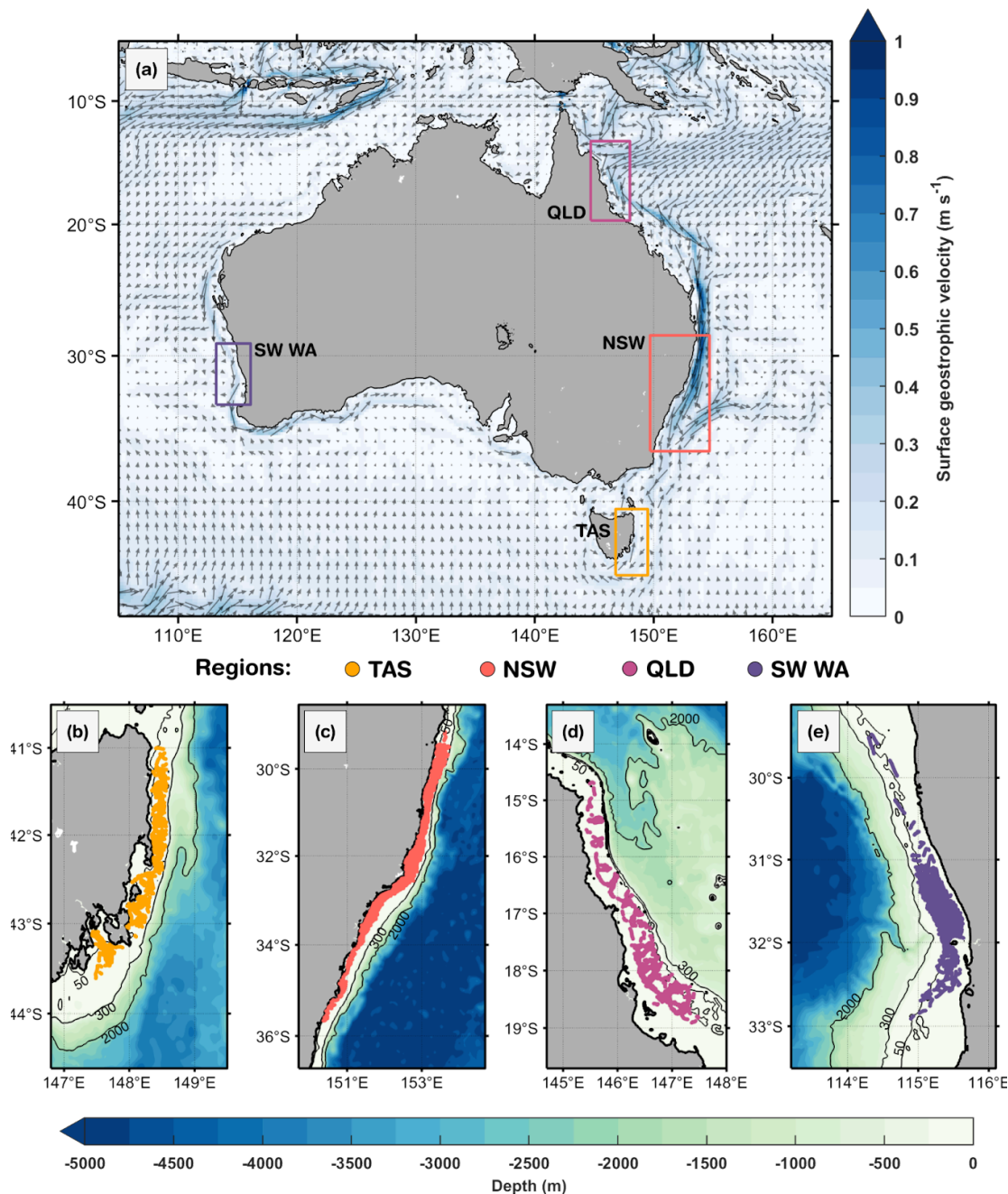


Figure 1. Study regions off the Australian coast. (a) Mean surface geostrophic currents (arrows) and highlighted boxes for each region of interest: northeastern Australia (Queensland region, QLD), southeastern Australia (New South Wales, NSW), southwest Western Australia (SW WA) and eastern Tasmania (TAS). Gliders' profile positions are illustrated in each sub-region: (b) TAS, (c) NSW, (d) QLD and (e) SW WA. In (a), the annual mean geostrophic currents were based on 1993 to 2020 and provided by the Integrated Marine Observing System (IMOS, <https://imos.aodn.org.au/oceancurrent>). Isobaths of 50 m, 300 m, and 2,000 m are shown in (b-e), derived from ETOPO1 bathymetry (Eakins & Sharman, 2010). Glider profiles are located over the continental shelf, in waters shallower than 200 m isobath..

200 2.4 Profile selection and data processing

201 Glider deployments were selected to keep only those profiles within the aforementioned study regions, spanning a
202 16-year period from January 2009 to June 2025. To ensure the quality of our analyses, the following quality control
203 steps were taken for each glider mission: (i) selection of only ‘good data’ flags (Woo & Gourcuff, 2023)⁴; (ii)
204 removal of chlorophyll outliers; (iii) applying a step to address non-photochemical quenching in chlorophyll
205 observations; and (iv) removal of data points inside the bottom boundary layer (BBL). To remove the noise from the
206 chlorophyll measurements (step (ii)), the outliers were identified based on a moving average of window size
207 equivalent to 1,000 points along the glider sampling, discarding values above two standard deviations of the
208 logarithmic chlorophyll. Moreover, light-induced fluorescence leads to errors in sensor measurements of
209 phytoplankton concentration (quenching), causing high variability in chlorophyll-a fluorescence profiles. To mediate
210 this effect (step (iii)), we used only night-time data points, defined as any time before sunrise or after sunset (as in
211 Schaeffer et al., 2016b). Regarding the variable BBL contamination due to sloping topography, we removed data
212 within 20 m above the seabed, similar to Schaeffer et al. (2014, 2017). This threshold aims to minimize
213 contamination from interference in the near-bottom levels when aggregating the shelf profiles over various
214 topographic depths for a combined analysis.

215

216 This study is focused on continental shelf waters, and hence the few measurements from deeper regions were
217 excluded. The continental shelf width and depth at the shelf-edge varies over each region. Off QLD and SW WA,
218 only measurements over bathymetry between 40 and 80 m were retained. For regions with deeper and steeper
219 continental shelves, i.e. TAS and NSW, we retained measurements between 50 and 120 m. Finally, we separated the
220 data points into downward and upward casts, binned each cast into a 1 m vertical resolution, averaged each pair of
221 down/upward casts, and binned the averaged profiles into fixed distances of 1 km horizontal resolution, which is
222 more than the median distance between profiles (e.g. 100–200 m in NSW region, Schaeffer et al., 2016b). These last
223 steps enable vertical and horizontal consistency of profiles, avoid glider’s direction bias when averaging the
224 down/upward casts, and reduce noise for shelf-scale comparison of subsurface MHW signals. In Fig. S1, we
225 illustrate a glider mission before and after quality control steps mentioned above.

226

227

4

228 https://content.aodn.org.au/Documents/IMOS/Facilities/Ocean_glider/Delayed_Mode_QAQC_Best_Practice_Manual_OceanGliders_LATEST.pdf

230 2.5 Classifying MHW vs non-MHW profiles

231 We classify MHW and non-MHW glider profiles by first collocating MHW severity index in time and space using
232 the satellite SST dataset. Thus, the severity index (S) was calculated for each profile following Sen Gupta et al.
233 (2020), as below:

$$234 \quad S_{i,d} = \frac{SST_{i,d} - SST_{i,d}^{clim}}{SST_{i,d}^{PC90} - SST_{i,d}^{clim}} \quad (1)$$

235 where $SST_{i,d}^{clim}$ is the long-term daily mean SST on the d th day of the year at location i , $SST_{i,d}^{PC90}$ is the 90th percentile
236 of SST on the same day and location as the glider profile. The MHWs were categorised into four types: (i) moderate,
237 $1 < S \leq 2$; (ii) strong, $2 < S \leq 3$; (iii) severe, $3 < S \leq 4$, and (iv) extreme ($S > 4$) following the category indices
238 proposed in Hobday et al. (2018). For each study region, the mean location of the glider profiles was determined,
239 and time series of the severity index were derived, enabling the representation of an ‘average’ severity timeline for
240 each region (see Figs. 1b-e).

241

242

243 2.6 In situ subsurface parameters

244 To further characterise the surface-MHWs in subsurface layers, some proxies were used, such as: (i) mixed layer
245 depth (MLD); (ii) thermocline depth; (iii) buoyancy frequency, i.e. degree of stratification; (iv) dissolved oxygen
246 saturation; (v) MHW depth extent, defined as depth containing 90% of the vertical heat content anomaly; (vi) depth
247 of maximum stratification, defined as the depth at which the buoyancy frequency reaches its maximum value in the
248 water column; and (vii) depth of deep chlorophyll maxima (DCM). For anomaly calculations in the subsurface, we
249 use non-MHW profiles as our baseline, i.e. anomalies are calculated relative to the mean non-MHW profile. This
250 provides a physically consistent background state and avoids potential bias introduced by uneven sampling of MHW
251 and non-MHW profiles. Therefore, we define the seasonal mean composite for each region as the average
252 non-MHW profiles over 3-month seasonal periods (austral summer - December/January/February, autumn -
253 March/April/May, winter - June/July/August, and spring - September/October/November).

254

255 The MLD was computed for each individual temperature profile by identifying the shallowest depth at which the
256 absolute temperature difference from the surface (0 m) exceeded a fixed threshold of 0.2° C. This threshold-based
257 method is commonly applied to in situ observations due to its physical relevance in stratified ocean conditions (e.g.,
258 de Boyer Montégut et al., 2004). Profiles with missing surface data or insufficient vertical resolution near the surface
259 were excluded from MLD calculations. MLD estimates were then averaged seasonally and grouped into MHW and
260 non-MHW categories, based on the presence or absence of MHW conditions.

261

262 The thermocline depth was computed from the vertical temperature profiles by calculating the temperature gradient
263 with respect to depth. The depth corresponding to the maximum negative gradient (i.e. the strongest rate of
264 temperature decrease with depth) was defined as the thermocline depth.

265

266 The buoyancy frequency, also called the Brunt Väisälä frequency, represents the degree of stratification and is
267 defined as:

$$268 \quad N^2 = -\frac{g}{\rho_0} \frac{\partial \rho}{\partial z} \quad (2)$$

269 where ρ_0 represents the background density, g is the gravitational constant and $\frac{\partial \rho}{\partial z}$ denotes the vertical gradient of
270 potential density. The density was calculated from the glider's vertical temperature and salinity profiles.

271

272 Dissolved oxygen saturation was computed from temperature, salinity and pressure following standard solubility
273 formulations, using the García and Gordon (1992) equation for seawater. Hence, oxygen saturation was calculated as
274 the ratio between measured dissolved oxygen concentration and the corresponding solubility value at in situ
275 conditions. This provides a temperature- and salinity-adjusted measure of oxygen availability relative to atmospheric
276 equilibrium, making it a useful indicator of both biogeochemical processes (production and respiration) and physical
277 transport mechanisms (vertical mixing and horizontal advection) that influence oxygen independently of solubility
278 changes.

279

280 MHW depth extent is defined as the depth which contains 90% of the vertical heat content anomaly, following
281 Elzahaby and Schaeffer (2019). For each MHW profile, positive temperature anomalies ($\Delta T > 0$) are integrated
282 vertically, and the depth extent corresponds to 90% of the profile's cumulative temperature anomaly. This approach
283 provides a physically consistent estimate of the vertical penetration of the MHW-associated warming relative to
284 background (non-MHW) conditions.

285

286 To evaluate the relationships between physical and biogeochemical variables during MHWs, we calculated the
287 correlations by regions and seasons separately. The variables considered include MHW depth extent, depth of
288 maximum stratification, depth of DCM, thermocline depth, dissolved oxygen (DO) anomalies, chlorophyll (CHL)
289 anomalies, and temperature anomalies above and below the MLD. Several restrictions were applied to ensure that
290 the correlations were unbiased.

- 291 (a) Only stratified profiles were retained, when the profile maximum buoyancy frequency (N^2) exceeded the
292 75th percentile of the regional distribution of maximum N^2 values. This approach excludes homogeneous
293 and weakly stratified profiles, often present in winter, that would otherwise give false strong correlations.
294 (b) Profiles lacking any positive subsurface temperature anomalies, since some of these metrics are undefined
295 in these cases and their inclusion would bias correlations toward spurious zero-inflation.

296 (c) Depths shallower than 5 m and within 5 m from the bottom were excluded to avoid surface and
 297 near-bottom artefacts.

298 (d) Correlations were considered significant only if the p-value was less than 0.05 and the number of data
 299 points was greater than 30 (Fig. S8).

300

301 2.7 Summary of glider missions

302 Across the four study regions, a total of 202 glider missions were recorded over the continental shelf between
 303 January 2009 and June 2025, with the highest number off SW WA (77 glider missions) and NSW (56 missions),
 304 followed by TAS (41 missions) and QLD (27 missions). These missions yielded 61,280 profiles (Table 1), with
 305 NSW and SW WA contributing the largest to the dataset (19,785 and 19,355 profiles, respectively), and fewer
 306 profiles in TAS (11,699) and QLD (10,441). These glider missions and their associated profiles were distributed
 307 seasonally, with and without MHW encounters (Table 1, Figs. 2b, d, f, h). Note that the number of chlorophyll
 308 profiles is lower than for other variables because of (i) quality control steps, (ii) removal of chlorophyll outliers and
 309 (iii) fluorescence quenching as described in sect. 2.4, and these data are presented in Supplementary Table S1.

310

311 **Table 1. Seasonal number of profiles with and without MHWs by region, as northeastern Australia (Queensland region,**
 312 **QLD), southwest Western Australia (SW WA), southeastern Australia (New South Wales, NSW) and eastern Tasmania**
 313 **(TAS).**

		Number of profiles				
		Summer (DJF)	Autumn (MAM)	Winter (JJA)	Spring (SON)	Total profiles
TAS	MHW	499	1,007	31	150	11,699
	Non MHW	1,450	2,535	2,181	3,846	
	Total	1,949	3,542	2,212	3,996	
NSW	MHW	294	989	342	1,167	19,785
	Non MHW	2,019	3,283	4,675	7,016	
	Total	2,313	4,272	5,017	8,183	
QLD	MHW	788	2,269	894	619	10,441
	Non MHW	1,697	953	1,300	1,921	
	Total	2,485	3,222	2,194	2,540	
SW WA	MHW	953	512	187	139	19,355
	Non MHW	3,751	4,251	5,611	3,951	

	Total	4,704	4,763	5,798	4,090	
--	--------------	--------------	--------------	--------------	--------------	--

314

315 NSW recorded the greatest number of MHW missions, with 12 separate glider deployments encountering MHW
316 conditions in spring and 10 in autumn (Fig. 2d), corresponding to 1,167 and 989 MHW profiles, respectively (Table
317 1). In SW WA, most missions and profiles occurred in winter and autumn, yet MHW missions (profiles) were more
318 frequent in summer (10 MHW gliders; 953 MHW profiles) and autumn (7 MHW gliders; 512 MHW profiles) (Fig.
319 2h, Table 1). TAS also recorded the highest number of MHW profiles in autumn (1,007 profiles, over 7 missions)
320 and summer (499 profiles, over 5 missions) (Fig. 2b, Table 1). In contrast, QLD showed missions with a more even
321 seasonal spread (Fig. 2f; Table 1), with MHW gliders and profiles more common in winter (5 missions; 894 profiles)
322 and autumn (5 missions; 2,269 profiles), this last season being the greatest number of MHW profiles among all
323 seasons and regions. Despite an overall lower number of MHW missions in QLD, the proportion of MHW profiles
324 relative to the total profiles was higher compared to other regions (Figs. 2e, g, Table 1). This reflects the fact that
325 MHWs in QLD are longer-lasting (Fig. 3h), and therefore glider deployments are more likely to capture them.

326

327 The vertical distribution of glider profiles also varied across regions due to distinct sloping topography (Figs. 2a, c,
328 e, g), with the highest profile density extending to depths of up to 100 m off TAS and NSW, while profiles were
329 generally shallower (mostly less than 60 m) off QLD and SW WA. MHW profiles, although consistently fewer than
330 non-MHW profiles, were more frequent in the upper 20 m (Figs. 2a, c, e, g) than at the surface or at deeper layers.
331 To ensure a robust representation of the vertical structure, profiles were truncated at depths where less than 10% of
332 profiles were available (and 20% for QLD and SW WA), resulting in a maximum analysed depth of 90 m for NSW
333 and TAS, 40 m for QLD, and 30 m for SW WA.

334

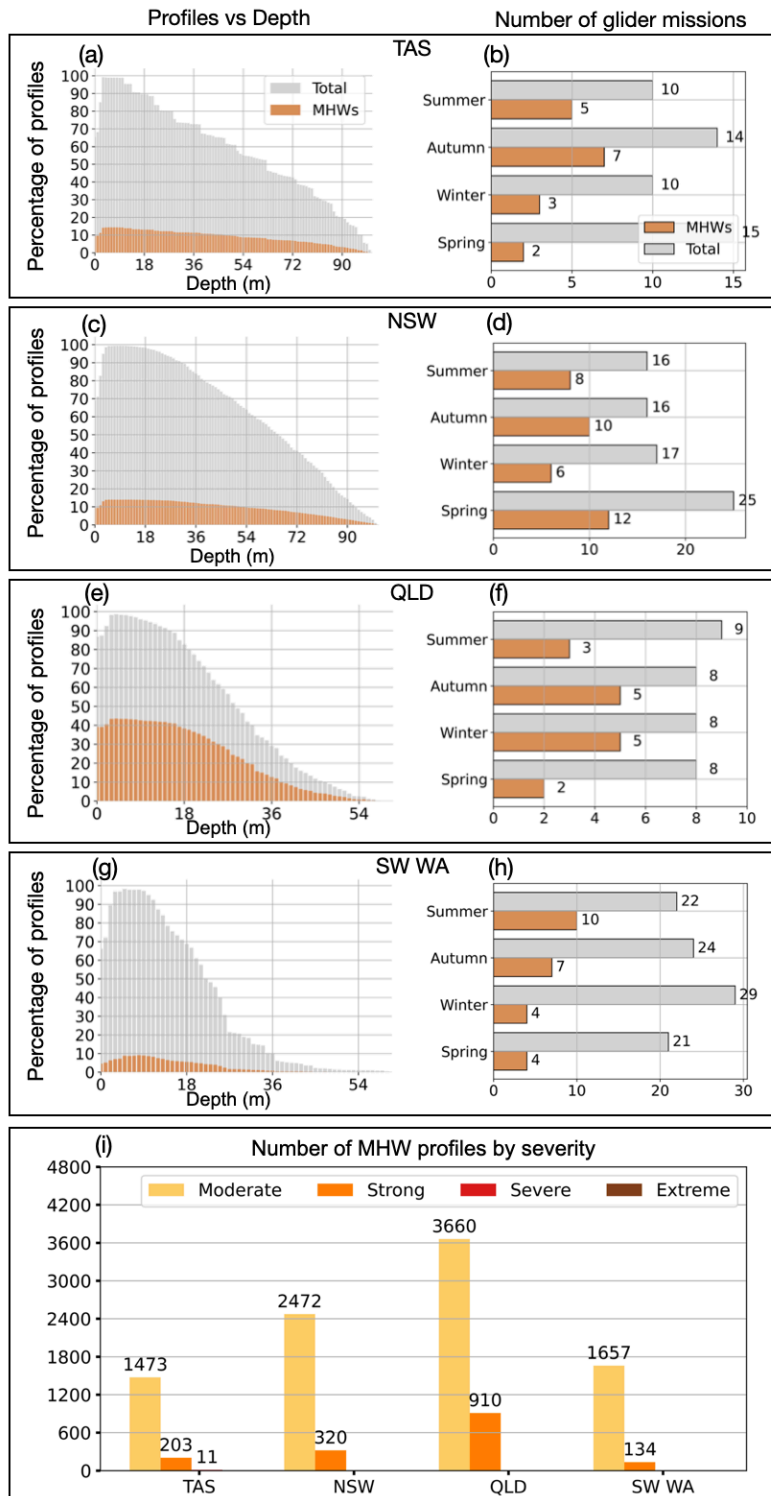
335 The severity of MHW profiles further highlighted regional differences (Fig. 2i). Most events were classified as
336 Category 1 (“Moderate”), with the highest numbers recorded in QLD (3660 profiles) and NSW (2472 profiles).
337 Category 2 (“Strong”) MHWs were most frequently sampled off QLD with 910 profiles, followed by 320 profiles
338 off NSW, 203 profiles off TAS, and 134 profiles off SW WA. Category 3 (“Severe”) events were few and only
339 sampled off TAS (11 profiles), while Category 4 (“Extreme”) events were not sampled over the continental shelf
340 after quality control steps. Together, these patterns reflect regional contrasts in the number of glider missions, the
341 seasonal and vertical distribution of profiles, and the severity of MHW conditions observed.

342

343

344

345



346

347 Figure 2. (a,c,e,g) Depth distribution of profiles for Tasmania (TAS), New South Wales (NSW), Queensland (QLD) and
 348 southwest Western Australia (SW WA), showing the percentage of total profiles (grey) and MHW profiles (orange) at
 349 each depth. (b,d,f,h) Seasonal counts of glider missions for each region, with total missions in grey and MHW missions in
 350 orange. (i) Number of MHW profiles per region, classified by severity: moderate, strong, severe and extreme. A glider is

351 classified as being in a MHW based on its position and whether a surface MHW was identified there from the NOAA
352 CoralTemp v3.1 SST with a reference period of 1985-2014.
353

354 3. Results

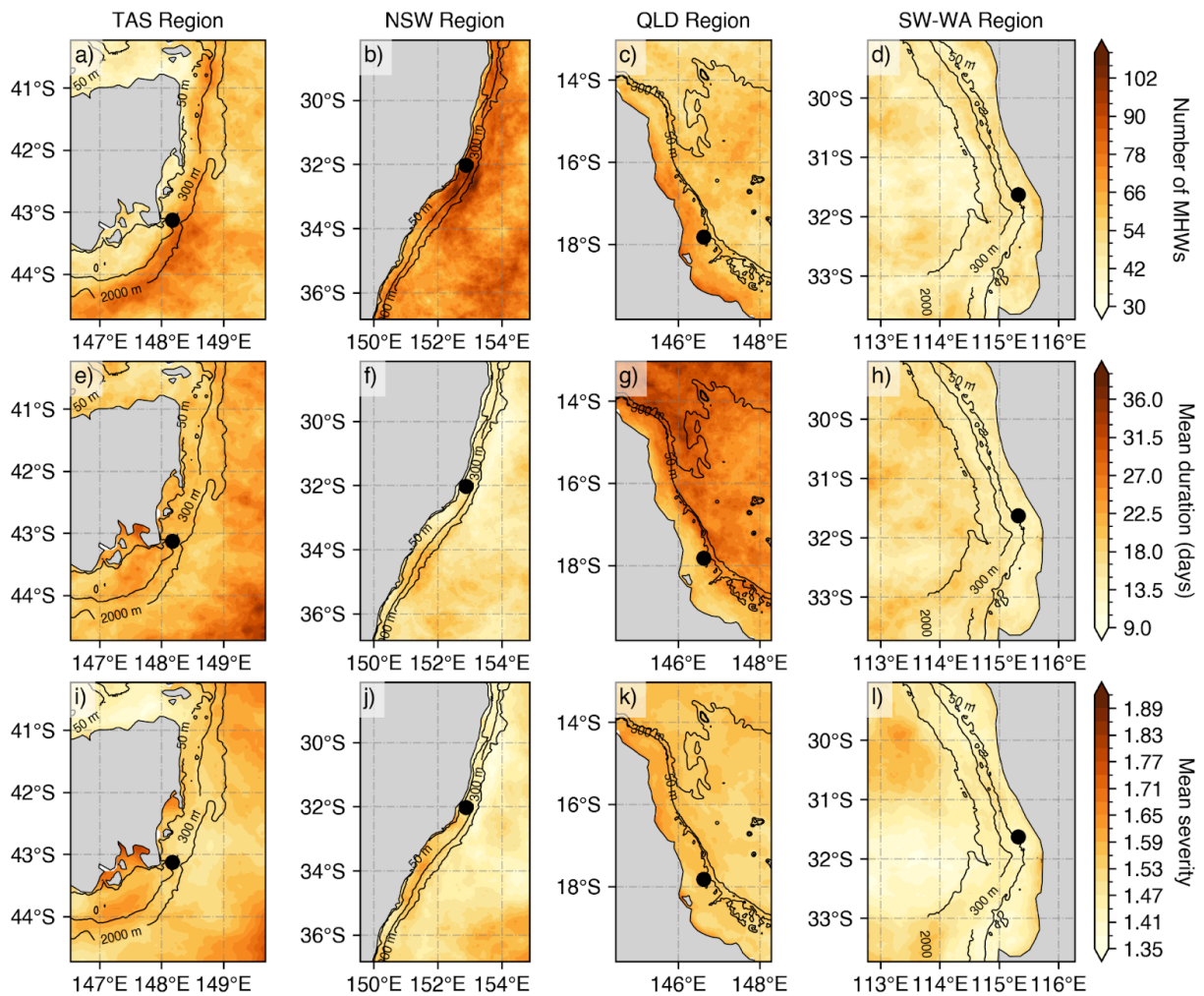
355 3.1 Characteristics of surface marine heatwaves

356 Regional variations in surface MHW metrics derived from satellite SST are illustrated in Fig. 3. From 2009 to
357 mid-2025, the eastern TAS region experienced over 80 surface MHWs (Fig. 3a), whereas fewer than 40 events were
358 detected along the continental shelf. Around Storm Bay in southeast TAS (43° S, 147.5° E), where most gliders were
359 initially deployed, MHWs were generally long-lasting with mean durations of 27-31 days and mean severity
360 exceeding 1.80 (Figs. 3e, i). To better capture the temporal distribution of MHWs relative to glider sampling, a
361 timeline analysis was performed for each region (Fig. 4). MHWs in the TAS region were most frequent from
362 November through to April, with strong to severe events concentrated between January and February (Fig. 4a). In
363 several instances, glider profiles sampled prolonged, strong to severe (Fig. 2i) MHWs, with severity indices
364 exceeding 3, including April 2016, February 2019, January 2022, and December 2023 (Fig. 4a).

365

366 Relative to other Australian regions, NSW exhibited the highest occurrence of MHWs, with more than 100 MHWs
367 detected over the study period (Fig. 3b). This highly dynamic region is typically characterised by short-lived MHWs
368 lasting less than 10 days (Fig. 3f). On the continental shelf, the mean severity of MHWs in NSW did not exceed
369 1.65, which is lower than that observed off TAS. However, two short-lived but severe events in September 2013, and
370 October 2018 (Fig. 4b), exceeded a severity index of 3. Glider missions deployed during these periods sampled
371 through the tail of the events, capturing a maximum severity value of 2.1 and 1.6, respectively.

372



373

374 Figure 3. Mean surface MHW metrics based on NOAA CoralTemp v3.1 (climatology 1985-2014 reference period) over the
 375 gliders' deployment period (1 January 2009 - 30 June 2025) by regions: (a-e-i) eastern Tasmania (TAS), (b-f-j)
 376 southeastern Australia (New South Wales, NSW), (c-g-k) Queensland region (QLD), and (d-h-l) southwest Western
 377 Australia (SW WA). The top panels represent the number of MHWs, the middle panels show the mean duration (in days),
 378 and bottom panels indicate the mean MHW severity. MHW severity values are calculated from selected SST pixels (black
 379 point) representative of the glider study regions off TAS (148.175° E, 43.125° S), NSW (152.575° E, 32.025° S), QLD
 380 (146.625° E, 17.825° S) and SW WA (115.325° E, 31.625° S).

381

382

383 Off northeast Australia (north of 20°S), MHWs were more frequent over the continental shelf, with 66-78
 384 occurrences recorded, compared to fewer events in offshore waters (waters deeper than 200-300 m isobaths Fig. 3c).
 385 MHWs on the continental shelf were shorter in duration (Fig. 3g), whereas offshore events were generally more
 386 prolonged, lasting 28–36 days on average. Across the central to northern Great Barrier Reef (GBR) off QLD, the

387 severity of MHWs typically had mean values below 1.65. However, there have been events with longer duration and
388 higher severity over the continental shelf, particularly between autumn and winter, in the past decade (Fig. 4c).
389 These intense seasonal events also coincided with a higher proportion of MHW gliders during these seasons (Fig.
390 2g). The 2016 MHW stood out as a prolonged (more than 5 months) and severe event captured by three glider
391 missions that sampled the onset (maximum severity: 2.6), middle (maximum severity: 2.3) and tail (maximum
392 severity: 2.6) of the event. Additional severe MHWs were also sampled in March 2017 (maximum severity: 2.9) and
393 September 2022 (maximum severity: 2.1). It is important to note that while some deployments shown in Fig. 4
394 coincided with severe satellite-detected MHWs, several profiles were excluded during quality control, and therefore
395 may not fully reflect peak severity of the event.

396

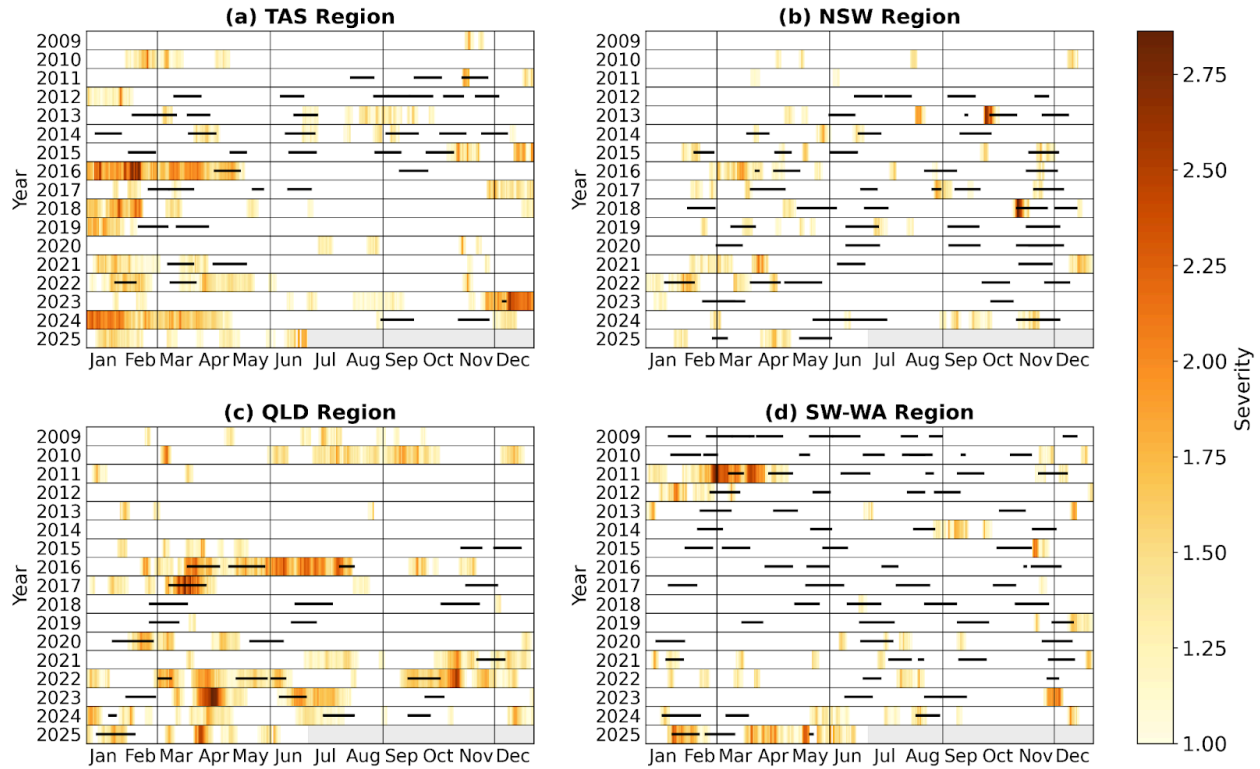
397 In contrast to eastern Australia, MHWs off the SW WA were shorter (less than 10 days on average; Fig. 3k), less
398 frequent with less than 45 MHWs recorded (Fig. 3j) and generally weaker in severity ranging between 1.3-1.5 (Fig.
399 3l). The low severity of MHWs in SW WA appears to be influenced by periods of sustained MHW cold spells off
400 the west coast, which contributed to the lower mean values over the study period (Feng et al., 2021). Such prolonged
401 and cold events can dampen the long-term mean MHW metrics, while other regions in eastern Australia experience
402 a higher prevalence of MHWs with greater duration and intensity. As indicated by the number of glider missions and
403 MHW profiles (Fig. 2h and Table 1), events in SW WA were more frequent and severe between summer and autumn
404 (Fig. 4d). While routine missions are conducted throughout the year, targeted MHW deployments are more likely to
405 occur during summer and autumn, when ocean temperatures are highest and MHW risk is elevated. Increased glider
406 sampling efforts may contribute to increased in situ observations of MHWs during these seasons, although the
407 seasonal peak in MHWs is also evident in the satellite record (Fig. 4d), indicating that the pattern is not only due to
408 sampling effort. The prolonged 2011 MHW is a key event in the region marked by strong to extreme severity
409 nearshore. This event was sampled by two glider missions, one in March (maximum severity: 2.1) and the other in
410 April (maximum severity: 1.6). More recently, in early 2025, SW WA experienced another prolonged, moderate to
411 strong MHW in the region which was also sampled by two glider missions at two critical stages: during the peak
412 (maximum severity: 2.2) and decline (maximum severity: 1.4) of the event, capturing the different phases of the
413 event.

414

415 These glider observations were critical, not only in validating satellite-derived MHW metrics across regions and
416 seasons, but also in offering detailed subsurface insights beyond satellite capabilities.

417

418



419

420 **Figure 4. Occurrence and severity of MHWs from January 2009 to June 2025 for (a) Tasmania (TAS), (b) New South**
 421 **Wales (NSW), (c) Queensland (QLD) and (d) southwest Western Australia (SW WA), with horizontal black lines**
 422 **indicating periods when glider missions occurred. Light gray bars in 2025 indicate times beyond the study period. Vertical**
 423 **grey lines delineate seasons.**

424

425 3.2 Marine heatwave severity influences on chlorophyll concentrations and dissolved oxygen

426 This section examines the impact of surface MHW severity on both surface and subsurface changes in chlorophyll
 427 concentrations and DO levels from glider-sampled MHWs over the Australian continental shelf. Fig. 5 compares
 428 chlorophyll and DO distributions between non-MHW periods and MHW categories (moderate and strong), above
 429 and below the MLD, combining data across all regions. Above the MLD, non-MHWs display a broader chlorophyll
 430 fluorescence distribution compared to MHWs, whereas below the MLD, the probability distributions show minimal
 431 variations. DO, on the other hand, shows distinct shifts in probability densities under MHW conditions, with
 432 multimodal peaks apparent both within and below the MLD, reflecting underlying regional and seasonal variations.

433

434 Within the mixed layer, chlorophyll concentrations generally decrease during MHWs (Fig. 5a; thick curves)
 435 compared to non-MHW conditions. Non-MHW conditions show a peak around 0.7 mg m^{-3} , whereas moderate
 436 MHWs peak near 0.25 mg m^{-3} , and strong MHWs around 0.23 mg m^{-3} , indicating progressively stronger decrease of
 437 chlorophyll concentrations in the MLD under increasing MHW severity. Below the MLD, non-MHW conditions

438 show lower subsurface chlorophyll ($\sim 0.25 \text{ mg m}^{-3}$) compared to within the mixed layer, with a slightly more
439 right-skewed distribution (dashed black; Fig. 5c). Moderate MHWs (yellow curve) do not show a significant change
440 in subsurface chlorophyll ($\sim 0.25 \text{ mg m}^{-3}$) from non-MHWs. In contrast, strong MHWs exhibit a peak around 0.6 mg
441 m^{-3} (orange curve; Fig. 5c), reflecting elevated subsurface concentrations.

442

443 For DO above the MLD, non-MHW periods show a bimodal distribution with the two main peaks at approximately
444 180 and $220 \text{ } \mu\text{mol kg}^{-1}$, suggesting the presence of two types of oxygen regimes (Fig. 5b). The first peak near 220
445 $\text{ } \mu\text{mol kg}^{-1}$ remains stable across non-MHW, moderate and strong severity. Under strong MHWs, the multi-modal
446 structure remains, but the density between 185 – $195 \text{ } \mu\text{mol kg}^{-1}$ is enhanced relative to non-MHW conditions, while
447 density above $230 \text{ } \mu\text{mol kg}^{-1}$ is reduced. Additionally, a third peak appears near $165 \text{ } \mu\text{mol kg}^{-1}$ during strong MHWs,
448 which may reflect localized depletion of DO. These changes indicate that strong MHWs alter the structure of DO
449 distribution above the MLD, indicating that strong MHWs are associated with a higher frequency of low-oxygen
450 values above the MLD and a relative reduction of high-oxygen values, although the multi-modal structure largely
451 reflects regional and seasonal regimes. As shown in Fig. S2, spring and summer exhibit generally higher mixed
452 layer DO compared to autumn, particularly in TAS and NSW, contributing to higher DO peak ($\sim 220 \text{ } \mu\text{mol kg}^{-1}$). In
453 contrast, QLD, which has the largest number of MHW profiles (Fig. 2i), tends to show lower mixed layer DO (Fig.
454 S2), contributing more strongly to intermediate and lower DO density ranges.

455

456 For DO below the MLD (Fig. 5d), the distributions slightly shift toward lower oxygen values under all conditions
457 compared to the layer above. During non-MHW periods, two peaks are observed at approximately 175 and 215
458 $\text{ } \mu\text{mol kg}^{-1}$. Under moderate MHWs, the distribution collapses into a single dominant peak near $\sim 205 \text{ } \mu\text{mol kg}^{-1}$,
459 indicating a homogenization of oxygen conditions below the MLD. Strong MHWs display an elevated lower peak at
460 $180 \text{ } \mu\text{mol kg}^{-1}$, similar to above the MLD, and a slightly reduced higher peak around $205 \text{ } \mu\text{mol kg}^{-1}$. Overall, the
461 response of DO to the severity of MHWs appears more heterogeneous and does not follow a uniform leftward shift.

462

463 Given that the results combine all regions and seasons, they may mask important regional and seasonal differences,
464 as well as sampling compositions. The following sections analyse the vertical profiles of surface MHWs across
465 study regions and seasons to better understand their subsurface impacts on biogeochemical variables.

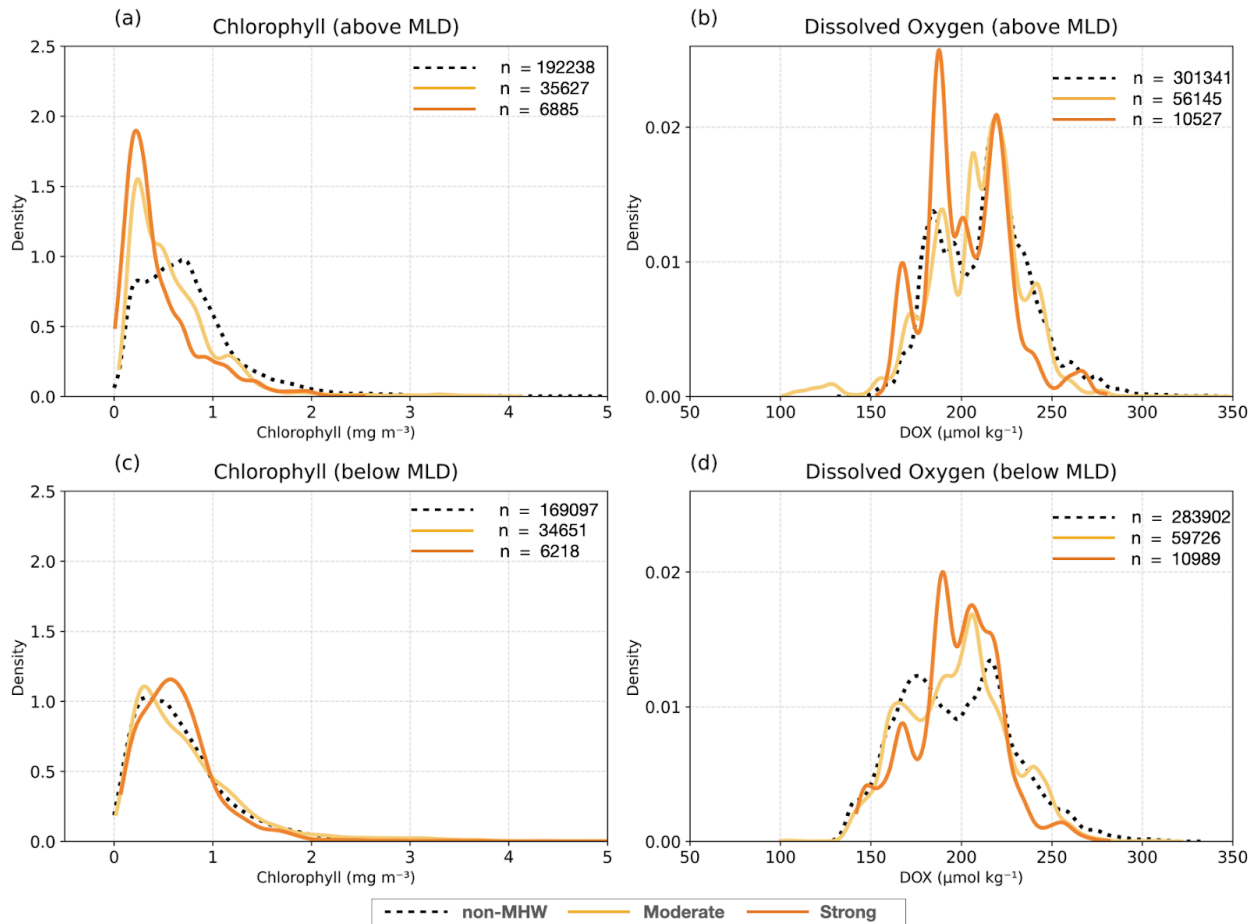
466

467

468

469

Probability density function of chlorophyll and dissolved oxygen



470

471 Figure 5. Probability density function of (a, c) chlorophyll fluorescence (mg m^{-3}) and (b, d) dissolved oxygen ($\mu\text{mol kg}^{-1}$)
 472 above and below the MLD respectively, during MHWs (thick lines) for all regions. The distribution of chlorophyll and
 473 dissolved oxygen during MHWs are shown with severity index (S) categories: $1 < S \leq 2$ (Category 1: moderate; yellow
 474 curve), and $2 < S \leq 3$ (Category 2: strong; orange curve), while non-MHW ones are in black ($S \leq 1$; dashed curve). The
 475 number of samples (n) are indicated.

476

477 3.3 Regional and seasonal changes in the water column

478 The vertical temperature structure of surface MHWs provides insight into how these events penetrate below the
 479 surface and interact with stratification and the mixed layer. These physical changes in the MLD, stratification, and
 480 MHW depth extent provide the context for examining chlorophyll variations throughout the water column and for
 481 assessing the depth of the DCM in particular seasons and regions. Changes in stratification directly affect
 482 phytoplankton productivity and oxygen concentrations, making it important to investigate how DO responds to
 483 MHWs alongside chlorophyll. In general, DO is highest at the surface due to diffusion from the atmosphere,

484 decreasing with depth, and also varies with temperature through solubility. This vertical perspective sets the stage
485 for comparing regional and seasonal patterns, to assess whether chlorophyll and DO responses to MHWs are
486 consistent across Australia's continental shelf and how they are shaped by local seasonal oceanographic conditions
487 (Figs. 6-9).

488

489 3.3.1 Eastern Tasmania region: eddy-rich and a convergence zone

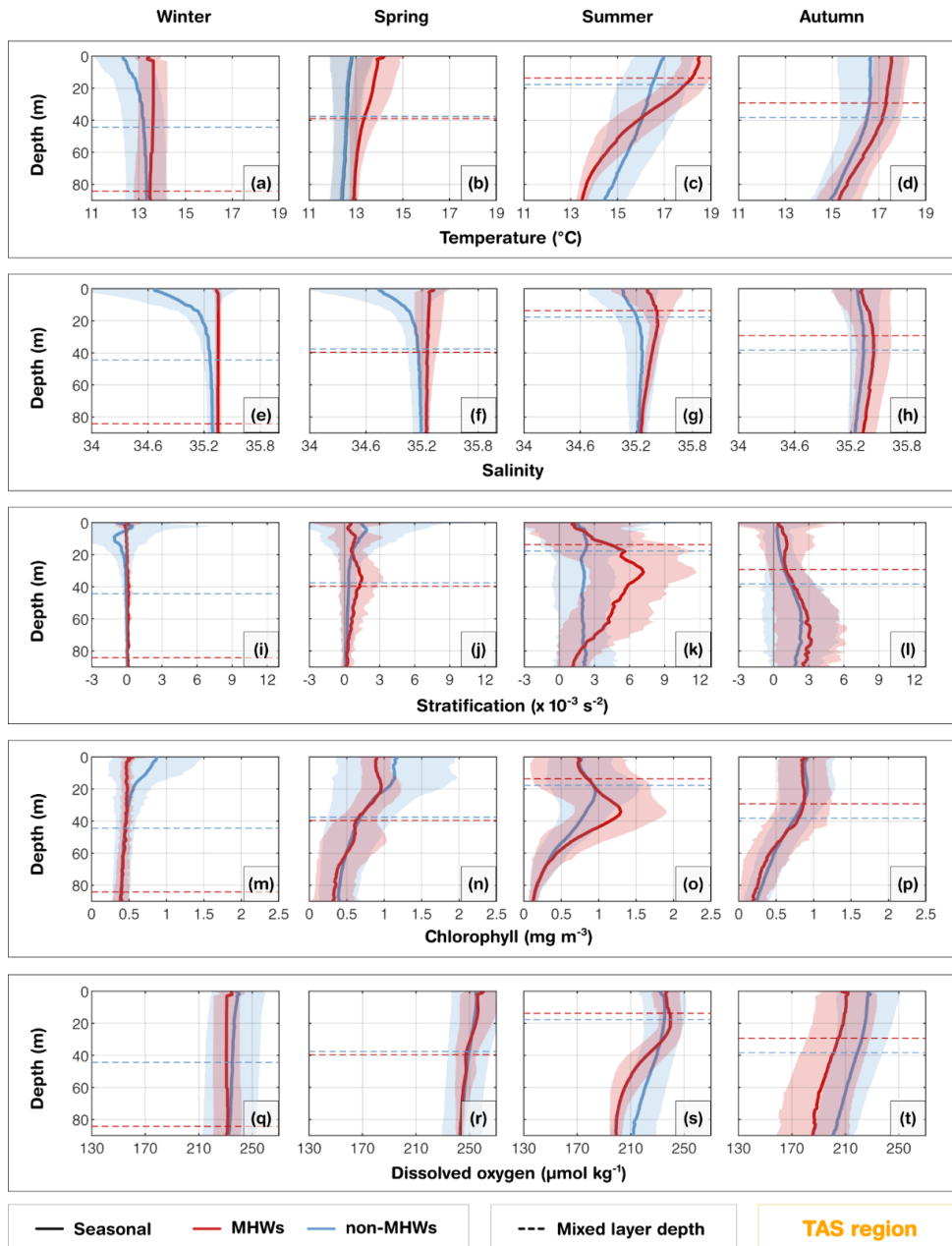
490 Waters off eastern Tasmania (TAS) experience the convergence of warm, salty, and nutrient-poor subtropical waters
491 from the southern extension of the East Australian Current (EAC) and cooler sub-Antarctic waters which lead to
492 complex oceanographic conditions along the continental shelf. The intensification and southward extension of the
493 EAC in the last few decades, associated with changes in the wind stress curl (Hill et al., 2008) and downstream
494 propagating mesoscale eddies (Stammer et al., 2006), has altered stratification and vertical mixing (Holbrook and
495 Bindoff, 1997; Ridgway, 2007; Oliver et al., 2017; Chiswell, 2023). This EAC extension and presence of eddies
496 can, in fact, induce MHWs and have implications for biogeochemical processes and overall ecosystem functioning
497 (Zhao et al., 2022; Chiswell, 2023). From the glider observations, the vertical structure of temperature, salinity,
498 chlorophyll and DO varied strongly within the seasons (Fig. 6). In the TAS region, glider profiles extended down to
499 about 90 m and showed pronounced seasonal cycles in MLD and MHW depth extent. During summer MHWs, the
500 MLD shoaled to about 18 m in summer (Fig. 6c), shallower than the seasonal composite mean MLD of non-mhws,
501 but extended to the bottom of the water column in winter (Fig. 6a). A similar pattern was reflected in the MHW
502 depth extent, which decreased to about 27 m in summer (Fig. S7) and deepened substantially in the other seasons
503 (~66 m in spring; ~ 44 m in winter and autumn; using method D in Fig. S7). The pronounced seasonality
504 corresponded to variations in stratification, which peaked at about $7 \times 10^{-3} \text{ s}^{-2}$ near 30 m during summer (Fig. 6k),
505 but was nearly absent in winter (Fig. 6i) and weakly stratifies in spring and autumn (Figs. 6j, l). Meanwhile, salinity
506 values were consistently higher during MHWs all year round and throughout the water column compared to the
507 seasonal mean composites derived from non-MHW conditions (Figs. 6 e-h). This indicates that during MHWs, the
508 shelf is influenced by warmer, saltier subtropical water masses associated with a strengthened or southward-shifted
509 EAC, similar to conditions observed during the 2015/2016 Tasman Sea MHW (Oliver et al., 2017). The increased
510 presence of these waters enhances upper-ocean density stratification, particularly in summer, which inhibits vertical
511 mixing with the cooler, fresher sub-Antarctic waters. This is in agreement with the strong and statistically significant
512 correlation ($r = 0.94$; Fig. 10) observed between MHW depth extent and the depth of maximum stratification during
513 summer in TAS region.

514

515 Summer MHWs were marked by reduced chlorophyll at the surface relative to the seasonal composites during
516 non-MHWs in the mixed layer (upper 20 m) but enhanced values at 40 m, exceeding 1.2 mg m^{-3} (Fig. 6o). During
517 summer, the deepening of the DCM corresponded closely to the MHW depth extent and the depth of maximum
518 stratification ($r = 0.40$; Fig. 10). In other seasons, weaker stratification limited the development of strong DCMs

519 both during MHWs and under non-MHWs conditions. The MHW profile of DO in summer (Fig. 6s) showed a
520 slightly higher concentration in the upper 35 m relative to the seasonal composite mean profile of non-MHWs,
521 exceeding 100% saturation within this layer (Fig. S3). This suggests enhanced oxygen production in the mixed layer
522 during MHWs, consistent with the strong DCM through photosynthesis (Fig. S3). Similarly, in spring, MHWs
523 showed slightly higher DO and saturation levels (> 100%) in the upper 25 m than under non-MHW conditions,
524 despite reduced chlorophyll. This suggests that oxygen variability was not controlled by phytoplankton biomass but
525 rather reflected supersaturation due to ventilation. In contrast, during autumn and winter, the oxygen saturation level
526 during MHWs was consistently lower than non-MHW conditions throughout the water column due to weak
527 stratification and reduced DCM, or through solubility loss due to warming (Fig. S3), all of which limit
528 phytoplankton productivity and oxygen production.

529



530

531 Figure 6. Tasmania region (TAS): Seasonal composite mean profiles of (a-d) temperature (°C), (e-h)
 532 stratification ($\times 10^{-3} s^{-2}$), (m-p) chlorophyll ($mg m^{-3}$) and (q-t) dissolved oxygen ($\mu mol kg^{-1}$) averaged for all MHW events
 533 (red), and non-MHW events (blue). Horizontal dashed lines indicate the corresponding seasonal composite mean MLDs
 534 for MHWs and non-MHWs. Shaded areas represent the respective standard deviations. Seasons are defined as winter
 535 (June-August), spring (September-November), summer (December-February), and autumn (March-May).

536

537 3.3.2 New South Wales region: narrow shelf and boundary current influence

538 In the New South Wales (NSW) region, the narrow continental shelf waters are shaped by the warm EAC, which
539 contributes to mixing and transports warm nutrient-poor waters onto the shelf when it meanders or shifts inshore.
540 The intrusions of the EAC increases the likelihood of full-depth extended MHWs, which are longer and dominant in
541 winter (Schaeffer et al., 2017, 2023). In this region, seasonal winds and stratification also strongly influence MHWs'
542 depth structure and development, especially in summer (Schaeffer and Roughan, 2017). In the glider observations,
543 during MHWs, warm anomalies were confined to slightly shallower depths (~35 m; Fig. S7) in winter and (~33 m;
544 Fig. S7) autumn, compared to deeper depths in austral summer (~47 m; Fig. S7) and spring (~46 m; Fig. S7).
545 Salinity showed no significant change during MHWs and remained relatively stable throughout the water column
546 throughout the year (Figs. 7e-h). Although waters off NSW are generally more stratified in summer than winter,
547 stratification further intensified and deepened during MHWs in all seasons, reaching $\sim 12 \times 10^{-3} \text{ s}^{-2}$ at 30-40 m in
548 summer and $\sim 3 \times 10^{-3} \text{ s}^{-2}$ at 45 m in winter, closely matching the depth extent of MHWs (Figs. 7i,k; S7; 10).

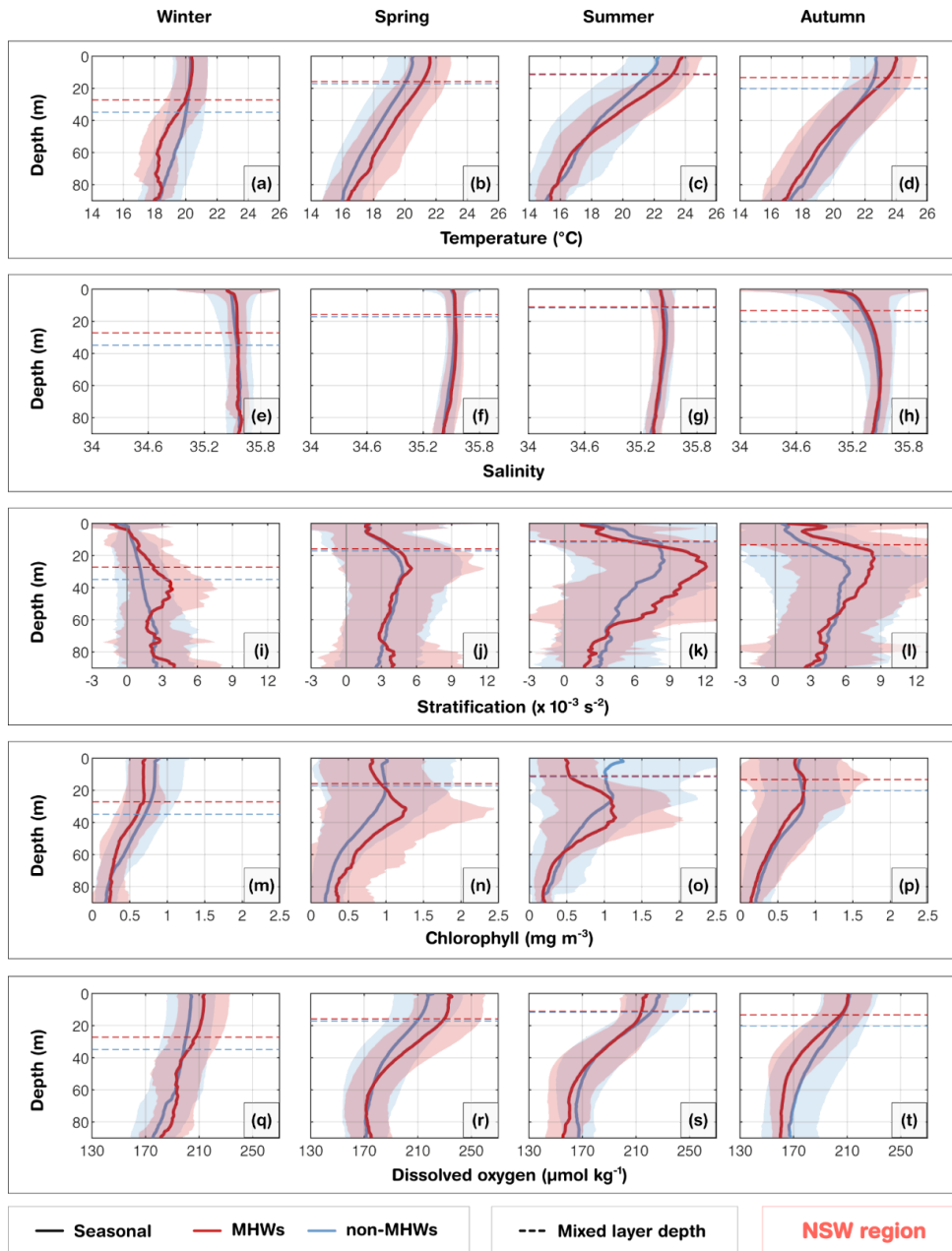
549

550 The DCM experienced strong seasonality. Across all seasons, surface chlorophyll concentrations were reduced
551 during MHWs, while increasing at ~20-40 m (exceeding 1 mg m^{-3}) during spring, summer and autumn (Figs. 7n-p).
552 These chlorophyll maxima were deeper and stronger than under non-MHW conditions, and their depth aligned well
553 with both maximum stratification and the MHW depth extent (Fig. S7). In contrast, during winter, weaker
554 stratification corresponded to shallower or absent DCMs, with chlorophyll concentrations below 1 mg m^{-3} (Figs.
555 7m).

556

557 In summer, MHWs were associated with reduced DO in the upper 20 m, likely due to warming-induced reduced
558 solubility (Fig. S3). At intermediate depths, a more pronounced DCM was present (Fig. 7o). Further deoxygenation
559 below 50 m may result from enhanced respiration of sinking organic matter from the intermediate layer. However,
560 little difference in DO levels from non-MHW conditions in the intermediate layer indicated that photosynthesis was
561 insufficient to alter the total mean DO (Fig. S3). Conversely, in spring, MHWs were associated with higher DO
562 concentrations in the upper 50 m, exceeding 100% saturation relative to non-MHW conditions within the mixed
563 layer (Fig. S3). This DO enhancement during spring is consistent with strong stratification and deep DCM (Figs.
564 7j,n,r), and is likely driven by photosynthesis, mixing or advection of oxygen-rich waters. Moreover, north-eastward
565 winds in spring (Wood et al., 2016), favour downwelling of warmer surface waters, contributing to the deep extent
566 of MHWs in spring (Fig. 7b) and transporting oxygen to deeper layers. By contrast, in autumn, DO concentrations
567 were similar within the mixed layer but decreased below the MLD (Fig. 7t), consistent with a DCM positioned
568 higher in the water column (Fig. 7l).

569



570

571 Figure 7. Same as Fig. 6, but for the New South Wales (NSW) region.

572

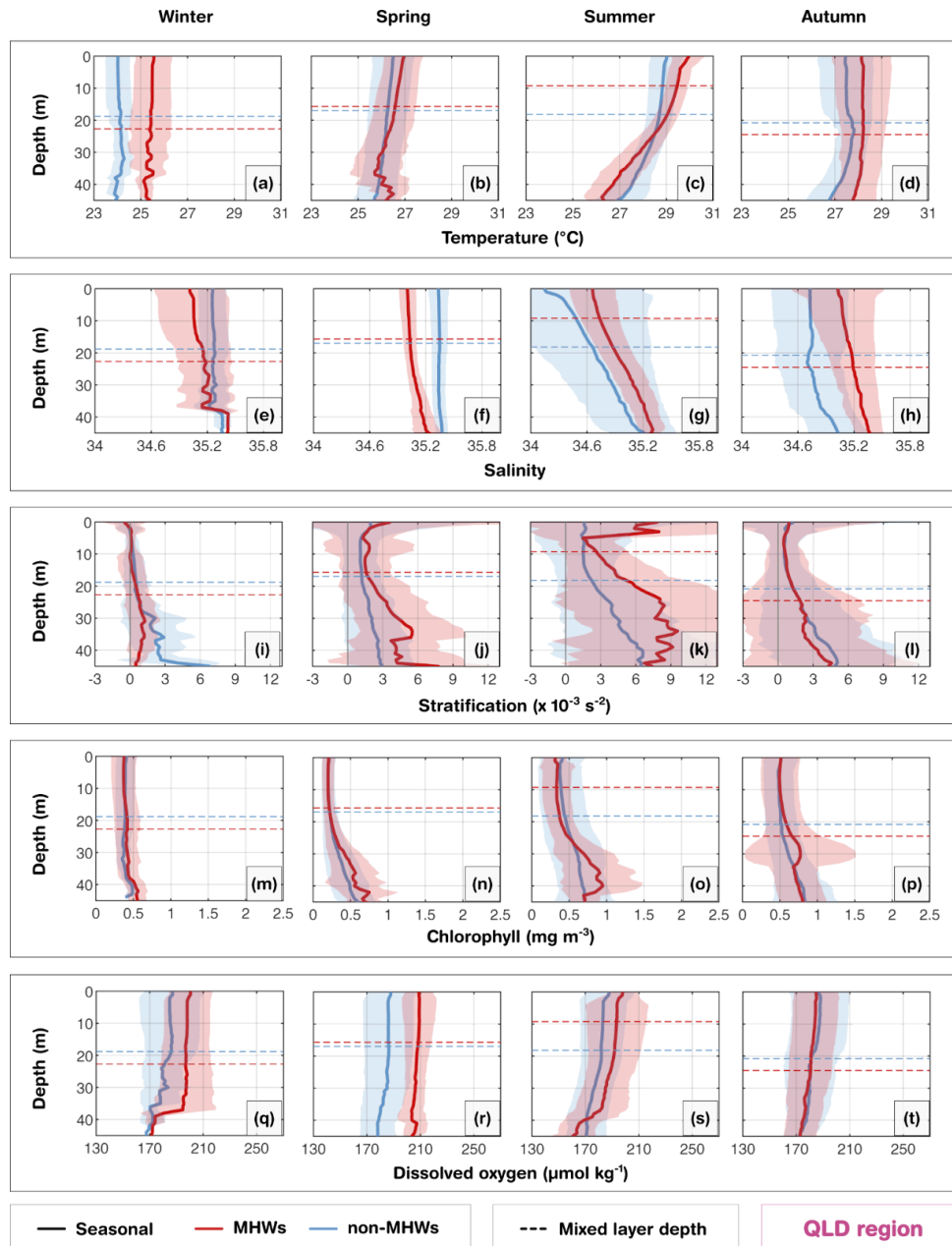
573 3.3.3 Queensland region: shallow shelf and biologically active area

574 The Queensland (QLD) region is home to the GBR, which has a shallow continental shelf with coral reefs and reef
 575 passages and the shelf circulation is influenced by the Gulf of Papua Current (in the north), East Australian Current
 576 (EAC; from the central sector to south), the Coral Sea circulation, riverine inputs and wind-driven processes
 577 (Ridgway et al., 2018; Benthuisen et al., 2022; Wolanski and Kingsford, 2024). The seasonal composite mean of

578 MLD and the MHW depth extent largely followed the seasonal cycle (Figs. 8; S7). During summer MHWs, the
579 MLD shoaled to 9 m consistent with a shallow MHW depth extent (~19m; Fig. S7), and strong stratification peaking
580 above $9 \times 10^{-3} \text{ s}^{-2}$ at the surface (Fig. 8k). The intense near-surface stratification is likely exacerbated by the
581 formation of barrier layers during the wet season (Schroeder et al., 2012), where riverine freshwater input and
582 precipitation create a buoyant low-salinity lens (Fig. 8g) and subsurface intrusive upwelling through reef passages
583 brings saltier Coral Sea waters below (Benthuisen et al. 2016). These barrier layers inhibit vertical mixing,
584 effectively trapping heat in the surface layer and intensifying the MHW magnitude. In contrast, during winter and
585 autumn MHWs, the MLD deepened to 23 m and 25 m respectively, consistent with a deepening of the MHW depth
586 extent to about 22 m and 27 m respectively (Fig. S7). During these seasons, the stratification weakened to less than 3
587 $\times 10^{-3} \text{ s}^{-2}$. Although fresher waters were observed near the surface in winter and spring, salinity values were not as
588 low as in summer, and the vertical salinity gradient was not as pronounced as in summer and autumn, suggesting the
589 dominance of wind-driven and convective mixing in homogenizing the water column during these cooler seasons.

590

591 Biologically, the strong physical stratification during summer MHWs shaped the vertical chlorophyll structure. The
592 DCM reached 1 mg m^{-3} at 40 m (Fig. 8o), coinciding with strong fluctuations in stratification levels below 30 m,
593 acting as a productive interface where light and nutrient availability overlap. Although less pronounced than
594 summer, autumn also displayed high chlorophyll concentrations exceeding 0.9 mg m^{-3} at 30 m. However,
595 chlorophyll concentration during MHWs in the upper 20 m remained lower than the seasonal composites, indicating
596 reduced productivity in the upper layers. The increased chlorophyll pattern observed in the subsurface layer may
597 reflect the seasonal transition toward weaker stratification and associated nutrient entrainment sustaining subsurface
598 productivity from deeper waters during the autumn MHWs. In contrast, winter and spring MHWs showed a weaker
599 coupling between stratification and chlorophyll than the other seasons, consistent with enhanced mixing. The DO
600 during MHWs compared to non-MHW conditions were consistently higher throughout the shallow water column
601 (except in autumn). This presents a counterintuitive thermodynamic behaviour, as warmer water typically holds less
602 dissolved gas. Consequently, the observed DO increase during summer, and spring indicates that biological oxygen
603 production (photosynthesis) was sufficient to offset the physical solubility loss induced by warming (Fig. S3). While
604 biological production dominates the summer signal, the higher DO observed during MHWs in winter may be related
605 to seasonal ventilation that drives the deep vertical extent of temperature anomalies, leading to higher oxygen levels
606 than normal. In contrast, the lower DO levels in autumn, despite the presence of subsurface chlorophyll, appears to
607 be dominated by enhanced respiration rates, consuming oxygen as organic matter from prior blooms. In addition to
608 enhanced respiration, reduced nutrient availability following summer could limit primary production, thereby
609 decreasing oxygen supply.



610

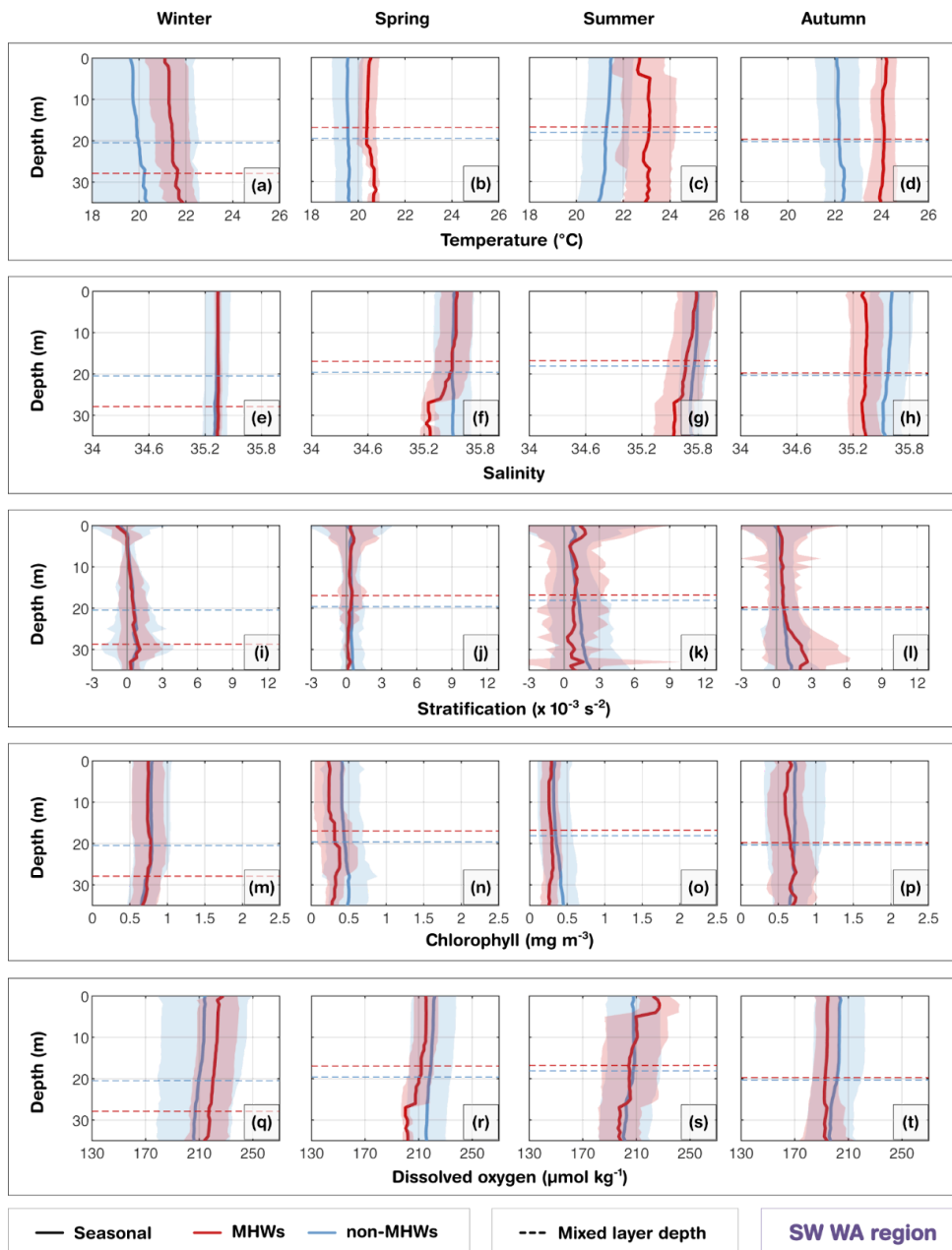
611 Figure 8. Same as Fig. 6, but for the Queensland (QLD) region.

612

613 3.3.4 Southwest Western Australia region: shallow shelf and oligotrophic conditions

614 The southwest Western Australia (SW WA) region is characterised by a shallow shelf dominated by the warm, fresh
 615 poleward-flowing Leeuwin Current, maintaining oligotrophic conditions, while the Capes Current emerges inshore
 616 during spring and summer months with upwelling leading to phytoplankton blooms (Hanson et al., 2005, Feng et al.,
 617 2025). The gliders were sampled over this coastal region, where the shelf narrows from ~50 km to 20 km (Fig. 1e;

618 Brooke et al., 2010). From the coast to the mid-shelf, waters had weaker stratification in the upper 40 m (Figs. 9i-j)
619 compared with other regions, where the small temperature inversion in autumn and winter is consistent with an
620 annual climatology from nearby mooring measurements (Feng et al., 2025). Unlike the stratified systems in eastern
621 Australia, this weak stratification coupled with the dominance of the Leeuwin Current drives downwelling-favorable
622 conditions that facilitate the rapid vertical propagation of surface heat anomalies. As a result, during surface MHWs,
623 anomalously warm surface temperatures extended further deep in all seasons, following the seasonal cycle of the
624 MLD, leading to $\sim+1-2^{\circ}\text{C}$ differences in the mean temperature profiles compared with non-MHW conditions (Figs.
625 9a-d). The MLD shoaled during summer MHWs compared to non-MHW conditions, in contrast to a deepening
626 during winter MHWs. In autumn, the MHW conditions were warmer and fresher than non-MHWs, potentially in
627 part related to sampling during the 2011 Ningaloo Niño (Fig. 4d), when glider measurements were concentrated
628 around $31.5-32^{\circ}$ S. During this extreme event, low salinity anomalies were transported by the Leeuwin Current and
629 were some of the lowest recorded values since the 1950s (Feng et al., 2015). This highlights that severe MHWs in
630 this region are largely advection-driven events, where the transport of buoyant, low-salinity tropical waters enhances
631 the density contrast with offshore waters, further trapping heat against the coast.
632



633

634 Figure 9. Same as Fig. 6, but for the southwest Western Australia (SW WA) region.

635

636 Biogeochemically, the strong advective nature of these MHWs exerts a controlling influence on shelf productivity.

637 During surface MHWs, shelf waters had lower chlorophyll concentrations than non-MHWs (Fig. 9m-p). Surface

638 MHWs were associated with anomalously high oxygen saturation levels ($>100\%$), higher than non-MHW conditions

639 during summer and winter. In summer, this likely reflects biological production in the upper layers due to shallower

640 MLD while in winter, it may be partially influenced by enhanced ventilation (Fig. S3). Weak stratification facilitates

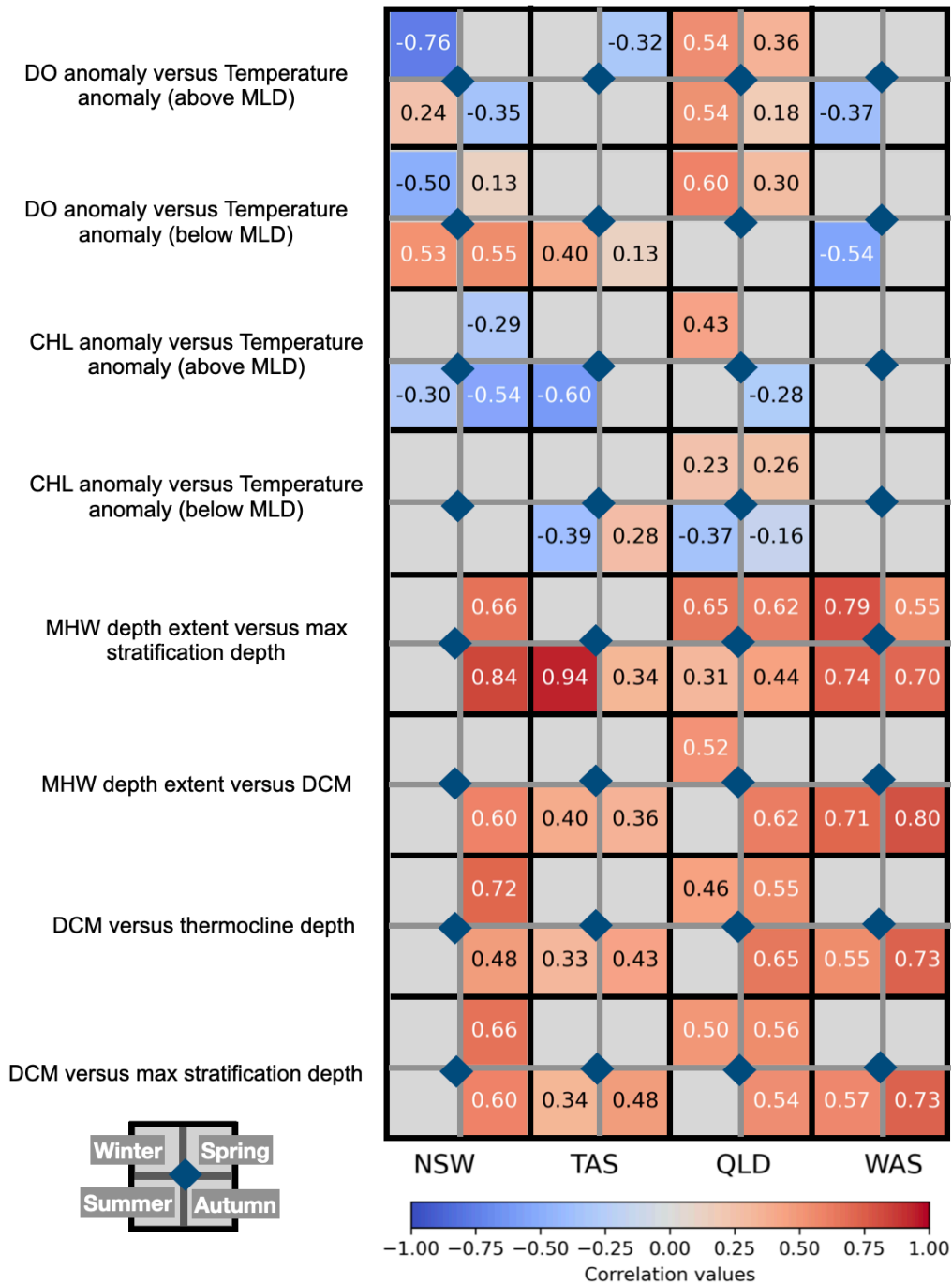
641 this supersaturation by allowing atmospheric oxygen to mix effectively throughout the water column, even if

642 dissolved oxygen is not substantially higher than non-MHW conditions. However, significantly lower DO levels
643 were observed in spring and autumn (Figs. 9r, t). In autumn, with sampling through the 2011 Ningaloo Niño, the
644 relatively reduced near-surface chlorophyll and DO might reflect equatorward influences on this region, as offshore
645 waters to the north have been recorded with lower chlorophyll and DO (e.g. Woo and Pattiaratchi, 2008; Weller et
646 al., 2011). This reduction suggests a decoupling from the solubility-driven pattern seen in other regions, pointing
647 instead to the physical advection of warm, nutrient-poor, and oxygen-depleted tropical waters by the intensified
648 Leeuwin Current, which suppresses local productivity and Capes Current upwelling. These results reveal that, in the
649 upper 40 m of coastal waters off SW WA, reduced stratification influences the vertical structure of chlorophyll and
650 DO (Fig. 10), even during surface MHWs, and they could be affected by latitudinal transport of water properties, as
651 has been found during MHWs caused by a Leeuwin Current intensification.

652

653

Significant correlations by regions (MHWs only)



654

655 Figure 10. Synthesis figure of seasonal correlations between key physical-biogeochemical variables during MHWs across
 656 four regions (NSW, TAS, QLD, SW WA). Rows correspond to variable pairs: (1) dissolved oxygen anomalies (DO) versus
 657 temperature anomalies (above the MLD), (2) dissolved oxygen anomalies (DO) versus temperature anomalies (below the
 658 MLD), (3) chlorophyll anomalies versus temperature anomalies (above the MLD), (4) chlorophyll anomalies versus
 659 temperature anomalies (below the MLD), (5) MHW depth extent versus depth of maximum stratification, (6) MHW

660 depth extent versus deep DCM depth, (7) DCM depth versus thermocline depth, and (8) DCM depth versus depth of
661 maximum stratification. Columns correspond to regions. Each cell is subdivided into four seasonal quadrants, colored by
662 the Pearson correlation coefficient (r) values with values indicated within each quadrant.

663

664

665 4. Discussion

666 MHWs have been extensively documented around Australia, yet their impact on subsurface biogeochemical
667 variables remains a critical gap in our understanding due to limited long-term observations. We used satellite SST
668 and up to 16 years of glider observations across four contrasting and well-observed coastal regions: eastern
669 Tasmania (TAS), New South Wales (NSW), Queensland (QLD), and southwest Western Australia (SW WA). Our
670 study reveals how surface MHWs alter, seasonally, the subsurface temperature, salinity, stratification, and
671 biogeochemical variables (chlorophyll and dissolved oxygen). These findings provide new insights into
672 region-specific responses, which help fill critical gaps in understanding the subsurface impacts of MHWs along the
673 continental shelf of Australia.

674

675 Across most regions, the vertical structure of temperature, salinity, and stratification displayed strong seasonality,
676 with shallow mixed layers and enhanced stratification in summer, and deeper, weaker stratification in winter. During
677 MHWs, these patterns tend to be intensified, with shallower MLD and stronger stratification in summer, and deeper
678 MLD in winter (except in NSW). During winter MHWs, the water column is already weakly stratified, and warming
679 alone does not generate a strong density gradient to shoal the MLD. In addition, anomalous processes associated
680 with winter MHWs, such as wind-driven mixing and horizontal advection, can further deepen the MLD relative to
681 typical winter conditions. In some regions, such as Western Australia, Leeuwin Current-driven MHWs produce deep
682 warming that can result in a deep MHW structure (Zhang et al., 2023), where warmer water penetrates to greater
683 depths, thereby leading to deeper MLD during MHW winters. In contrast, NSW did not exhibit this deepening of the
684 MLD during winter MHWs due to the hydrography of the EAC which dominates the NSW shelf year-round. Unlike
685 other regions, stratification in NSW is not driven purely by seasonal heating and cooling but is strongly modulated
686 by shelf encroachment of the EAC, mesoscale eddies, and current instabilities. This persistent influence also shapes
687 the seasonality of phytoplankton in NSW, with summer-spring biomass maxima and reduced winter abundance
688 (Schaeffer et al, 2015), consistent with our findings. SW WA exhibited particularly minimal stratification changes
689 due to its naturally well-mixed conditions, however, transient increases in stratification can occur during periods of
690 wind relaxation or fluctuations in the Leeuwin or Capes Currents. The MHW depth extent was shallower in strongly
691 stratified (summer) conditions and deeper during winter when the water column was more homogeneous. These
692 results align well with Schaeffer and Roughan (2017) and with hypothesis (3) that the vertical depth extent of
693 surface MHWs vary seasonally according to background stratification and hydrography.

694

695 Chlorophyll responses are tightly coupled to MHW severity and regional hydrography. Results showed that surface
696 chlorophyll above the MLD overall declines with increasing MHW severity, in line with previous studies (Le Grix et
697 al., 2020; Sen Gupta et al., 2020; Gruber et al., 2021). This finding supports hypothesis (4) that the severity of MHW
698 modulates chlorophyll concentration and is also consistent with hypothesis (1) that surface MHWs generally reduce
699 chlorophyll concentrations in the mixed layer. The observed decline in surface chlorophyll with increasing severity
700 is likely driven by enhanced stratification and reduced nutrient supply from the subsurface which limit surface
701 phytoplankton growth during MHWs. This pattern is evident in the correlation plots (Figs. 10 and S4), which reveal
702 an overall negative relationship between temperature and chlorophyll anomalies above the MLD, except in SW WA
703 where limited sampling may affect the correlation (Fig. S8).

704

705 Subsurface chlorophyll distributions during MHWs has been a topic of incipient discussion. Here, our study showed
706 evidence for increased chlorophyll below the MLD during strong MHWs along the Australian continental shelves,
707 pointing to the formation of a sharper and deeper DCM in spring, summer and autumn due to enhanced stratification
708 (except in the oligotrophic region of Western Australia). This finding supports hypothesis (2), indicating that despite
709 surface reductions, MHWs can promote deeper chlorophyll maxima and enhanced subsurface productivity. Although
710 the surface becomes nutrient-poor, the shoaling of the MLD during MHWs increases phytoplankton exposure to
711 higher light intensities, thereby allowing phytoplankton to thrive at depth (e.g. Hayashida et al., 2020). DCM depth
712 correlated strongly with the depth of maximum stratification in NSW (Pearson correlation coefficient, $r = 0.66$ in
713 spring, $r = 0.60$ in autumn), in TAS ($r = 0.48$ in autumn), in QLD ($r = 0.56$ in Spring) and SW WA ($r = 0.73$ in
714 autumn), all statistically significant. We also found strong correlations between DCM depth and MHW extent, in
715 NSW ($r = 0.60$ in autumn), QLD ($r = 0.62$ in autumn, $r = 0.52$ in winter) and SW WA ($r = 0.71$ in summer, $r = 0.80$
716 in autumn). This finding is consistent with Ma and Chen (2025), who showed that MHWs promote DCM
717 development at the global scale. In contrast, in winter or in vertically-mixed upper ocean waters, MHWs penetrate to
718 depth, eroding stratification and suppressing DCM. The level of stratification controls the thermocline depth, which
719 we found to be strongly correlated with DCM depth (Figs. 10 and S4), and thereby governs both the vertical position
720 of the DCM and the MHW depth extent. Our results support hypothesis (3) that regional hydrography and seasonal
721 stratification control the vertical extent of MHWs.

722

723 DO responses to MHW and their severity are less straightforward. Australia's surrounding waters exhibit distinct
724 oxygen regimes due to contrasting water masses, biogeochemical environments and seasonal variability.
725 Low-oxygen regimes are usually present in tropical and subtropical regions (Paulmier and Ruiz-Pino, 2009; Davila
726 et al., 2023) such as QLD and SW WA, influenced by oxygen-poor water masses, while high-oxygen regimes are
727 found in temperate regions (NSW, TAS), dominated by well-ventilated waters. During strong MHWs, low-oxygen
728 regimes may become further deoxygenated in the MLD (Figs. S2, S3), such as in QLD, due to enhanced
729 stratification and reduced vertical ventilation, consistent with hypothesis (1) that MHWs reduce dissolved oxygen in
730 the mixed layer and hypothesis (4) that MHW severity modulates dissolved oxygen variability. Although reduced

731 upwelling can limit the entrainment of oxygen-poor subsurface waters, it also restricts the supply of oxygen from
732 deeper layers and reduces mixing, isolating the mixed layer. In shallow coastal regions, elevated temperatures
733 further decrease solubility, and may increase the biological oxygen demand. Besides temperature's direct effect on
734 oxygen solubility, changes in DO arise from complex interactions between circulation and stratification, and primary
735 productivity (Gruber, 2011; Gruber et al., 2021).

736

737 Regional differences in DO distributions during MHWs illustrate these complex interactions due to circulation and
738 stratification, and primary production. In NSW and TAS, MHWs generally decrease DO in the MLD (except
739 summer NSW), consistent with lower oxygen saturation level than during non-MHWs (Fig. S3), due to the
740 temperature-dependent decrease in oxygen solubility (negative DO tendency with temperature in Figs. S5c).
741 However, below the MLD, localized oxygen increases occur particularly in summer, near subsurface chlorophyll
742 maxima (Figs.10, S5b,d). These seasonal increases may reflect enhanced biological production during which oxygen
743 is generated below the MLD through photosynthesis, or ventilation associated with the strong East Australian
744 Current (EAC) and its eddy-driven intrusions (Malan et al., 2020). In addition to these biophysical drivers, regional
745 wind patterns further modulate the vertical structure of DO during spring in NSW. North-eastward winds in spring
746 (Wood et al., 2016), favour downwelling of warmer surface waters, contributing to the deeper vertical extent of
747 MHWs and transporting oxygen to subsurface layers.

748

749 In QLD, DO responses to MHWs are linked to seasonal changes in stratification, mixing, and biological
750 productivity. During summer MHWs, strong near-surface stratification, reinforced by riverine freshening and
751 wet-season rainfall, creates a shallow MLD that traps heat and supports high biological activity. This results in
752 elevated DO throughout the upper water column, with oxygen saturation exceeding 100% in the MLD (Fig. S3),
753 indicating that photosynthesis more than compensates for the temperature-driven decline in oxygen solubility. This
754 finding is in agreement with hypothesis (2) that subsurface waters may experience enhanced oxygen concentrations
755 associated with deeper productivity. In contrast, autumn shows lower DO during MHWs compared to non-MHW
756 periods, although subsurface chlorophyll remains elevated. This reduction coincides with warmer and saltier
757 conditions that decrease oxygen solubility and combined with weaker stratification, facilitates the mixing of
758 low-oxygen waters upward. Enhanced respiration following the summer bloom may also deplete DO.

759

760 In SW WA, well-mixed waters in the upper 40 m exhibited relatively uniform DO profiles, with enhanced DO in
761 summer and winter oxygenation during MHWs. For example, in summer, the weakened and offshore-displaced
762 Leeuwin Current combined with strong southerly winds (Feng et al., 2025) promotes strong ventilation and
763 enhanced mixing. During autumn, anomalously warm, fresh waters with reduced chlorophyll in the upper 20 m and
764 reduced DO, compared with non-MHW conditions, indicate the potential influence for intensified Leeuwin Current
765 transport to affect biogeochemical variables during advection-driven MHWs (Pearce and Feng, 2013). Overall, the

766 study results indicate that stratification and primary productivity jointly regulate oxygen variability, with regional
767 hydrography determining whether MHWs enhance or suppress oxygenation across the water column.

768

769 While this study provides a comprehensive analysis of subsurface thermal and biogeochemical structure associated
770 with surface MHWs, several limitations related to sampling density should be acknowledged. Despite the
771 availability of 16 years of glider observations, sampling remains uneven across regions, depths and seasons, which
772 constrains the robustness of some composite profiles. In particular, subsurface properties during spring MHWs are
773 not robustly characterised in some regions due to the small number of captured events. For example, TAS in spring
774 are based on only two MHW events, limiting confidence in the seasonal mean of these profiles. Similarly, in QLD,
775 the number of MHW profiles during autumn exceeds that of non-MHW profiles, which may not give a true
776 representation of the seasonal mean.

777

778 Additional limitations arise from combining surface MHW detection based on daily, night-time, gap-filled satellite
779 data with sub-daily in situ glider observations, which may bring inconsistencies between both surface and
780 subsurface signals. Furthermore, the available dataset is insufficient to assess the influence of large-scale climate
781 modes on the subsurface structure of surface MHWs, and lack some biological parameters (e.g. nutrient
782 concentrations) which restricts the interpretation of DO and DCM. Addressing these limitations will require
783 high-resolution observations across all seasons and coordinated modelling efforts to develop robust subsurface
784 climatologies.

785

786 5. Conclusions

787 This study shows that the impacts of MHWs on dissolved oxygen and chlorophyll along the Australian continental
788 shelf depend strongly on regional hydrography, seasonal stratification, and, to some extent, event severity. Taken
789 together, our results show that surface-only perspectives underestimate the biogeochemical and potential ecological
790 impacts of MHWs. Subsurface glider observations revealed that MHWs can simultaneously suppress surface
791 productivity while intensifying subsurface production, with consequences for oxygen levels and food-web
792 dynamics, depending on regional hydrography and stratification. Stratification, which appears consistently enhanced
793 during summer MHWs, emerges as a useful proxy for the vertical extent of surface MHWs and on the DCM. These
794 findings underscore the importance of accounting for region-specific monitoring to manage ecological consequences
795 of MHWs.

796

797 The interaction between physical processes, such as seasonal circulation, stratification and biological feedback,
798 including deep chlorophyll maxima formation and oxygen production, highlights the complex biogeochemical
799 responses to MHWs. By leveraging up to 16 years of glider observations, this work demonstrates the importance of
800 sustained subsurface monitoring and coupled physical–biogeochemical approaches to better predict ecosystem

801 vulnerability. Future research is needed to transform sparse and high-frequency sampling of continental shelf waters
802 to develop coastal climatologies appropriate for assessing subsurface MHW impacts. Long-term measurements are
803 key to improving our understanding of MHWs' vertical structure, drivers, and ecological consequences and, in
804 combination with shelf modelling, can provide a holistic view of how they affect variability and extremes in our
805 coastal and shelf systems. These efforts are critical for managing the impacts of MHWs on marine ecosystems under
806 a warming climate.

807

808 **Data availability:** The glider data is publicly available through the Australian Ocean Data Network (AODN) Portal
809 at: <https://portal.aodn.org.au/search?uuid=c317b0fe-02e8-4ff9-96c9-563fd58e82ac> and
810 <https://thredds.aodn.org.au/thredds/catalog/IMOS/ANFOG/catalog.html>.

811 The NOAA CoralTemp v3.1 SST product is available at: <https://coralreefwatch.noaa.gov/product/5km/index.php>.

812 The IMOS OceanCurrent delayed-mode, gridded (adjusted) sea level anomaly product and surface geostrophic
813 velocity is available from 1993–2020 at:

814 <https://thredds.aodn.org.au/thredds/catalog/IMOS/OceanCurrent/GSLA/DM/catalog.html>, while the near-real-time
815 data is available at: <https://thredds.aodn.org.au/thredds/catalog/IMOS/OceanCurrent/GSLA/NRT/catalog.html>.

816

817 **Code availability:** Processed glider data and code can be accessed at
818 [https://github.com/GlidersMHWs/Subsurface-biogeochemical-marine-heatwaves-on-the-Australian-continental-shel](https://github.com/GlidersMHWs/Subsurface-biogeochemical-marine-heatwaves-on-the-Australian-continental-shelf/tree/main)
819 [f/tree/main](https://github.com/GlidersMHWs/Subsurface-biogeochemical-marine-heatwaves-on-the-Australian-continental-shelf/tree/main)

820 **Author contributions:** DM lead the project in assigning analysis and writing. JA and RLG assisted with data
821 reprocessing. AS designed and supervised the project. All authors contributed to the analyses, discussions, writing
822 and proofreading.

823 **Competing interests:** The authors declare that they have no conflict of interest.

824 **Acknowledgments:** We would like to acknowledge CLIVAR (Climate and Ocean – Variability, Predictability and
825 Change) 2023 Marine heatwave summer school, through which this project started. We also thank everyone who
826 was involved in the glider deployment, piloting, and processing, through the IMOS Ocean Gliders Facility led by
827 Prof. Charitha Pattiaratchi, as well as the IMOS Event Based Sampling national committee. All glider data were
828 sourced from Australia's Integrated Marine Observing System (IMOS) – IMOS is enabled by the National
829 Collaborative Research Infrastructure Strategy (NCRIS). It is operated by a consortium of institutions as an
830 unincorporated joint venture, with the University of Tasmania as Lead Agent.

831 **Financial support:**

832

833 FEKG. acknowledges funding from Canada's C150 Research Program (Grant No. 50296) and Schmidt Sciences,
834 LLC.

835

836 **References**

837 Amaya, D. J., Miller, A. J., Xie, S.-P., and Kosaka, Y.: Physical drivers of the summer 2019 North Pacific marine
838 heatwave, *Nat. Commun.*, 11(1), 1903, doi:10.1038/s41467-020-15820-w, 2020

839 Benthuisen, J., Feng, M., and Zhong L.: Spatial patterns of warming off Western Australia during the 2011
840 Ningaloo Niño: Quantifying impacts of remote and local forcing, *Cont. Shelf Res.*, 91, 232-246,
841 doi:10.1016/j.csr.2014.09.014, 2014.

842 Benthuisen, J. A., Tonin, H., Brinkman, R., Herzfeld, M., and Steinberg, C.: Intrusive upwelling in the Central
843 Great Barrier Reef. *J. of Geophys. Res.: Oceans*, 121(11), pp.8395-8416, doi:10.1002/2016JC012294, 2016.

844 Benthuisen, J. A., Oliver, E. C. J., Feng, M., and Marshall, A. G.: Extreme marine warming across tropical Australia
845 during austral summer 2015–2016, *J. Geophys. Res.: Oceans*, 123(2), 1301-1326, doi:10.1002/2017JC013326,
846 2018.

847 Benthuisen, J. A., Steinberg, C., Spillman, C. M., and Smith, G. A.: Oceanographic drivers of bleaching in the
848 GBR: from observations to prediction. Volume 4: Observations and predictions of marine heatwaves. Report to
849 the National Environmental Science Program. Reef and Rainforest Research Centre Limited, Cairns (47pp.).
850 Available at: <https://nesptropical.edu.au/index.php/round-4-projects/project-4-2/>, 2021.

851 Benthuisen, J. A., Emslie, M. J., Currey-Randall, L. M., Cheal, A. J. and Heupel, M. R.: Oceanographic influences
852 on reef fish assemblages along the Great Barrier Reef, *Prog. Oceanogr.*, 208, p.102901,
853 doi:10.1016/j.pocean.2022.102901, 2022.

854 Benthuisen, J. A., Pattiaratchi, C., Spillman, C. M., Govekar, P., Beggs, H., Bastos de Oliveira, H., Chandrapavan,
855 A., Feng, M., Hobday, A. J., Holbrook, N. J., Jaine, F. R. A., and Schaeffer, A.: Observing marine heatwaves
856 using ocean gliders to address ecosystem challenges through a coordinated national program. In *Frontiers in*
857 *Ocean Observing*. E.S. Kappel, V. Cullen, I.C.A. da Silveira, G. Coward, C. Edwards, P. Heimbach, T. Morris,
858 H. Pillar, M. Roughan, and J. Wilkin, eds, *Oceanogr.* 38(Supplement 1), doi:10.5670/oceanog.2025e101, 2025.

859 Berkelmans, R., & Oliver, J. K.: Large-scale bleaching of corals on the Great Barrier Reef. *Coral reefs*, 18(1), 55-60,
860 doi:10.1007/s003380050154, 1999.

861 Blondeau-Patissier, D., Gower, J. F. R., Dekker, A. G., Phinn, S. R., and Brando, V. E.: A review of ocean color
862 remote sensing methods and statistical techniques for the detection, mapping and analysis of phytoplankton
863 blooms in coastal and open oceans, *Prog. Oceanogr.*, 123, 123–144, doi:10.1016/j.pocean.2013.12.008, 2014.

864 Brooke, B., Creasey, J., and Sexton, M.: Broad-scale geomorphology and benthic habitats of the Perth coastal plain
865 and Rottneest Shelf, Western Australia, identified in a merged topographic and bathymetric digital relief model,
866 *Intern. J. Rem. Sens.*, 31(23), 6223–6237, doi: 10.1080/01431160903403052, 2010.

867 Capotondi, A., Rodrigues, R. R., Sen Gupta, A., Benthuisen, J. A., Deser, C., Frölicher, T. L., Lovenduski, N. S.,
868 Amaya, D. J., Le Grix, N., Xu, T., and Hermes, J.: A global overview of marine heatwaves in a changing climate,
869 *Commun. Earth Environ.*, 5, 701, doi:10.1038/s43247-024-01806-9, 2024.

870 Cavole, L. M., Demko, A. M., Diner, R. E., Giddings, A., Koester, I., Pagniello, C. M., ... and Franks, P. J.:
871 Biological impacts of the 2013–2015 warm-water anomaly in the Northeast Pacific: winners, losers, and the
872 future, *Oceanogr.*, 29(2), 273–285. doi:10.5670/oceanog.2016.32, 2016.

873 Chen, M., Pattiaratchi, C. B., Ghadouani, A., and Hanson, C.: Seasonal and inter-annual variability of water column
874 properties along the Rottneest continental shelf, south-west Australia, *Ocean Sci.*, 15, 333–348,
875 doi:10.5194/os-15-333-2019, 2019.

876 Chen, M., Pattiaratchi, C. B., Ghadouani, A. and Hanson C.: Influence of storm events on chlorophyll distribution
877 along the oligotrophic continental shelf off south-western Australia, *Front. Mar. Sci.*, 7, 287,
878 doi:10.3389/fmars.2020.00287, 2020.

879 Chen, Q., Li, D., Feng, J., Zhao, L., Qi, J., and Yin, B.: Understanding the compound marine heatwave and
880 low-chlorophyll extremes in the western Pacific Ocean, *Front. Mar. Sci.*, 10, 1303663,
881 doi:10.3389/fmars.2023.1303663, 2023.

882 Chiswell, S. M.: Tasman Sea high- and low- chlorophyll events, their links to marine heat waves, cool spells, and
883 global teleconnections, *New Zealand J. Mar. Fresh. Res.*, 57(4), 550–567, doi:10.1080/00288330.2022.2076702,
884 2023.

885 Davila, X., Olsen, A., Lauvset, S. K., McDonagh, E. L., Brakstad, A., and Gebbie, G.: On the origins of open ocean
886 oxygen minimum zones, *J. Geophys. Res.: Oceans*, 128(8), e2023JC019677, doi:10.1029/2023JC019677, 2023.

887 Davies, K. T.: Using passive acoustic monitoring from gliders for near realtime detection and dynamic management
888 of North Atlantic right whales (*Eubalaena glacialis*) in the Laurentian Channel Dynamic Shipping Zones, 2021.

889 Eakins, B. W., and Sharman, G. F.: Volumes of the World’s Oceans from ETOPO1. NOAA National Geophysical
890 Data Center, Boulder, CO, 7(1), 2010.

891 Elzahaby, Y., and Schaeffer, A.: Observational insight into the subsurface anomalies of marine heatwaves, *Frontiers*
892 *in Marine Science*, 6, doi:10.3389/fmars.2019.00745, 2019.

893 Feng, M., McPhaden, M. J., Xie, S.-P., and Hafner, J.: La Niña forces unprecedented Leeuwin Current warming in
894 2011, *Sci. Rep.*, 3(1), 1277, doi:10.1038/srep01277, 2013.

895 Feng, M., Benthuisen, J., Zhang, N., and Slawinski, D.: Freshening anomalies in the Indonesian throughflow and
896 impacts on the Leeuwin Current during 2010–2011, *Geophys. Res. Lett.*, 42(20), 8555–8562,
897 doi:10.1002/2015GL065848, 2015.

898 Feng, M., Caputi, N., Chandrapavan, A., Chen, M., Hart, A., and Kangas, M.: Multi-year marine cold-spells off the
899 west coast of Australia and effects on fisheries, *J. Mar. Sys.*, 214, 103473, doi:10.1016/j.jmarsys.2020.103473,
900 2021.

901 Feng, M., Bui, T., and Benthuisen, J. A.: Seasonal climatology of the Leeuwin Current-Capes Current system off
902 southwest Australia from long-term moored observations, *J. Geophys. Res.: Oceans*, 130(5), e2025JC022662,
903 doi:10.1029/2025JC022662, 2025.

904 Frölicher, T. L., Fischer, E. M. and Gruber, N.: Marine heatwaves under global warming, *Nature*, 560, 360–364,
905 doi:10.1038/S31586-018-0383-9, 2018.

906 Garcia, H. E., & Gordon, L. I.: Oxygen solubility in seawater: Better fitting equations. *Limnology and*
907 *oceanography*, 37(6), 1307-1312, doi:10.4319/lo.1992.37.6.1307, 1992.

908 Gomes, D. G., Ruzicka, J. J., Crozier, L. G., Huff, D. D., Brodeur, R. D., and Stewart, J. D.: Marine heatwaves
909 disrupt ecosystem structure and function via altered food webs and energy flux. *Nat. Commun.*, 15(1), 1988.
910 doi:10.1038/s41467-024-46263-2, 2024.

911 Great Barrier Reef Marine Park Authority, Australian Institute of Marine Science, and CSIRO.: Reef Snapshot:
912 Summer 2024–25, Reef Authority, Townsville, Available at: <https://hdl.handle.net/11017/4116>, 2025.

913 Gregory, C. H., Holbrook, N. J., Marshall, A. G., and Spillman, C. M.: Atmospheric drivers of Tasman Sea marine
914 heatwaves, *J. Climate*, 36(15), 5197-5214, doi:10.1175/JCLI-D-22-0538.1, 2023.

915 Gruber, N.: Warming up, turning sour, losing breath: ocean biogeochemistry under global change, *Phil. Trans. R.*
916 *Soc. A.*, 3691980, doi:10.1098/rsta.2011.0003, 2011.

917 Gruber, N., Boyd, P. W., Frölicher, T. L., and Vogt, M.: Biogeochemical extremes and compound events in the
918 ocean, *Nature*, 600, 395–407, doi:10.1038/s41586-021-03981-7, 2021.

919 Hanson, C. E., Pattiaratchi, C. B., and Waite, A. M.: Sporadic upwelling on a downwelling coast: phytoplankton
920 responses to spatially variable nutrient dynamics off the Gascoyne region of Western Australia, *Cont. Shelf Res.*,
921 25(12-13), 1561-1582, doi:10.1016/j.csr.2005.04.003, 2005.

922 Hayashida, H., Matear, R. J., and Strutton, P. G.: Background nutrient concentration determines phytoplankton
923 bloom response to marine heatwaves, *Glob. Change Bio.*, 26(9), 4800-4811, doi:10.1111/gcb.15255, 2020.

924 Hill, K. L., Rintoul, S. R., Coleman, R., and Ridgway, K. R.: Wind forced low frequency variability of the East
925 Australia Current, *Geophys. Res. Lett.*, 35(8), doi:10.1029/2007GL032912, 2008.

926 Hobday, A. J., & Pecl, G. T.: Identification of global marine hotspots: sentinels for change and vanguards for
927 adaptation action. *Reviews in Fish Biology and Fisheries*, 24(2), 415-425, doi:10.1007/s11160-013-9326-6,
928 2014.

929 Hobday, A. J., Alexander, L. V., Perkins, S. E., Smale, D. A., Straub, S. C., Oliver, E. C. J., Benthuisen, J. A.,
930 Burrows, M. T., Donat, M. G., Feng, M., and Holbrook, N. J.: A hierarchical approach to defining marine
931 heatwaves, *Prog. Oceanogr.*, 141, 227-238, doi:10.1016/j.pocean.2015.12.014, 2016.

932 Hobday, A. J., Oliver, E. C., Sen Gupta, A., Benthuisen, J. A., Burrows, M. T., Donat, M. G., ... and Smale, D. A.:
933 Categorizing and naming marine heatwaves, *Oceanogr.*, 31(2), 162-173, doi:10.5670/oceanog.2018.205, 2018.

934 Holbrook, N. J., and Bindoff, N. L.: Interannual and decadal temperature variability in the southwest Pacific Ocean
935 between 1955 and 1988, *J. Clim.*, 10(5), 1035-1049.
936 doi:10.1175/1520-0442(1997)010<1035:IADTVI>2.0.CO;2, 1997.

937 Holbrook, N. J., Hernaman, V., Koshiba, S., Lako, J., Kajtar, J. B., Amosa, P., and Singh, A.: Impacts of marine
938 heatwaves on tropical western and central Pacific Island nations and their communities, *Global and Planetary*
939 *Change*, 208, 103680, doi.org/10.1016/j.gloplacha.2021.103680, 2022.

940 Huang, Z., Feng, M., Dalton, S. J., and Carroll, A. G.: Marine heatwaves in the Great Barrier Reef and Coral Sea:
941 their mechanisms and impacts on shallow and mesophotic coral ecosystems, *Sci. Total Env.*, 908, 168063,
942 doi:10.1016/j.scitotenv.2023.168063, 2024.

943 IMOS 2025, “OceanCurrent - Gridded sea level anomaly - Delayed mode - DM02”,
944 [https://catalogue-imos.aodn.org.au/geonetwork/srv/eng/catalog.search#/metadata/da30c0b8-4978-4a26-915e-b80](https://catalogue-imos.aodn.org.au/geonetwork/srv/eng/catalog.search#/metadata/da30c0b8-4978-4a26-915e-b80c88bb4510)
945 [c88bb4510](https://catalogue-imos.aodn.org.au/geonetwork/srv/eng/catalog.search#/metadata/da30c0b8-4978-4a26-915e-b80c88bb4510), accessed August-2025.

946 Kwiatkowski, L., Torres, O., Bopp, L., Aumont, O., Chamberlain, M., Christian, J. R., ... & Ziehn, T.: Twenty-first
947 century ocean warming, acidification, deoxygenation, and upper-ocean nutrient and primary production decline
948 from CMIP6 model projections. *Biogeosciences*, 17(13), 3439-3470, doi:10.5194/bg-17-3439-2020, 2020.

949 Lachkar, Z., Lévy, M., and Smith, K. S.: Strong intensification of the Arabian Sea oxygen minimum zone in
950 response to Arabian Gulf warming. *Geophys. Res. Lett.*, 46(10), 5420–5429, doi:10.1029/2018GL081631, 2019.

951 Laufkötter, C., Zscheischler, J., and Frölicher, T. L.: High-impact marine heatwaves attributable to human-induced
952 global warming, *Science*, 369(6511), 1621–1625. doi:10.1126/science.aba0690, 2020.

953 Le Gendre, R., Varillon, D., Fiat, S., Hocdé, R., de Ramon N'Yeurt, A., Andréfouët, S., ... & Menkes, C.:
954 ReefTEMPS: the Pacific Islands coastal temperature network. *Earth System Science Data*, 17(10), 5277-5301,
955 doi:10.5194/essd-17-5277-202510.5194/essd-17-5277-2025, 2025.

956 Le Grix, N., Zscheischler, J., Laufkötter, C., Rousseaux, C. S., and Frölicher, T. L.: Compound high temperature and
957 low chlorophyll extremes in the ocean over the satellite period, *Biogeosci. Discussions*, 2020, 1-26.
958 doi:10.5194/bg-18-2119-2021, 2020.

959 Ma, X. and Chen, G.: Marine heatwaves are shaping the vertical structure of phytoplankton in the global ocean.
960 *Commun. Earth Environ.*, 6, 715, doi:10.1038/S33247-025-02718-y, 2025.

961 Malan, N., Archer, M., Roughan, M., Cetina-Heredia, P., Hemming, M., Rocha, C., ... and Queiroz, E.: Eddy-driven
962 cross-shelf transport in the East Australian Current separation zone, *J. Geophys. Res.: Oceans*, 125(2),
963 e2019JC015613, doi: 10.1029/2019JC015613, 2020.

964 Malan, N., Sen Gupta, A., Schaeffer, A., Zhang, S., Doblin, M. A., Pilo, G. S., ... and Spillman, C. M.: Lifting the lid
965 on marine heatwaves, *Prog. Oceanogr.*, 103539. doi:10.1016/j.pocean.2025.103539, 2025.

966 Marre, J. B., Thebaud, O., Pascoe, S., Jennings, S., Boncoeur, J., and Coglán, L.: The use of ecosystem services
967 valuation in Australian coastal zone management, *Marine Policy*, 56, 117-124,
968 doi:10.1016/j.marpol.2015.02.011, 2015.

969 Meier, H. M., Väli, G., Naumann, M., Eilola, K., and Frauen, C.: Recently accelerated oxygen consumption rates
970 amplify deoxygenation in the Baltic Sea, *J. Geophys. Res.: Oceans*, 123(5), 3227-3240,
971 doi:10.1029/2017JC013686, 2018.

972 Noh, K. M., Lim, H. G., and Kug, J. S.: Global chlorophyll responses to marine heatwaves in satellite ocean color.
973 *Environ. Res. Lett.*, 17(6), 064034, doi:10.1088/1748-9326/ac70ec, 2022.

974 Oliver, E. C., Benthuyesen, J. A., Bindoff, N. L., Hobday, A. J., Holbrook, N. J., Mundy, C. N., and
975 Perkins-Kirkpatrick, S. E.: The unprecedented 2015/16 Tasman Sea marine heatwave, *Nat. Commun.*, 8(1),
976 16101, doi:10.1038/ncomms16101, 2017.

977 Oliver, E. C., Benthuyesen, J. A., Darmaraki, S., Donat, M. G., Hobday, A. J., Holbrook, N. J., ... and Sen Gupta, A.:
978 Marine heatwaves, *Ann. Rev. Mar. Sci.*, 13(1), 313-342, doi:10.1146/annurev-marine-032720-095144, 2021.

979 Pattiaratchi, C., Hollings, B., Woo, M., and Welhena, T.: Dense shelf water formation along the south-west
980 Australian inner shelf, *Geophys. Res. Lett.*, 38, L10609, doi:10.1029/2011GL046816, 2011.

981 Pattiaratchi, C., Woo, L. M., Thomson, P. G., Hong, K. K., and Stanley, D.: Ocean glider observations around
982 Australia. *Oceanogr.*, 30(2), 90-91, doi:10.5670/oceanog.2017.226, 2017.

983 Paulmier, A. and Ruiz-Pino, D.: Oxygen minimum zones (OMZs) in the modern ocean.: *Prog. Oceanogr.*, 80(3-4),
984 113-128, doi:10.1016/j.pocean.2008.08.001, 2009.

985 Pearce, A., Lenanton, R., Jackson, G., Moore, J., Feng, M., and Gaughan, D.: The “marine heat wave” off Western
986 Australia during the summer of 2010/11, Fisheries Research Report No. 222, Department of Fisheries, Western
987 Australia. 40pp., Available at: https://www.fish.wa.gov.au/documents/research_reports/fr222.pdf, 2011.

988 Pearce, A. F. and Feng, M.: The rise and fall of the “marine heat wave” off Western Australia during the summer of
989 2010/2011, *J. Mar. Sys.*, 111, 139-156, doi:10.1016/j.jmarsys.2012.10.009, 2013.

990 Richardson, A. J., Savage, J., Coman, F., Davies, C., Eriksen, R., McEnnulty, F., Slotwinski, A., Tonks, M.,
991 Uribe-Palomino, J.: The impact on zooplankton of the 2011 heatwave off Western Australia. In Richardson, A.
992 J., Eriksen, R., Moltmann, T., Hodgson-Johnston, I., Wallis, J. R. (Eds). *State and trends of Australia’s ocean*
993 *Report*, doi:10.26198/5e16adc449e87, 2020.

994 Ridgway, K. R.: Long-term trend and decadal variability of the southward penetration of the East Australian
995 Current, *Geophys. Res. Lett.*, 34(13), doi:10.1029/2007GL030393, 2007.

996 Ridgway, K. R., Benthuyesen, J. A., and Steinberg, C.: Closing the gap between the Coral Sea and the equator: Direct
997 observations of the north Australian western boundary currents, *J. Geophys. Res.: Oceans*, 123(12), 9212-9231,
998 doi:10.1029/2018JC014269, 2018.

999 Ridgway, K. R. and Ling, S. D.: Three decades of variability and warming of nearshore waters around Tasmania,
1000 *Prog. Oceanogr.*, 215, 103046, doi:10.1016/j.pocean.2023.103046, 2023.

1001 Roberts, S. D., Van Ruth, P. D., Wilkinson, C., Bastianello, S. S., & Bansemer, M. S.: Marine heatwave, harmful
1002 algae blooms and an extensive fish kill event during 2013 in South Australia. *Frontiers in Marine Science*, 6,
1003 610, doi:10.3389/fmars.2019.00610, 2019.

1004 Rose, T. H., Smale, D. A., and Botting, G.: The 2011 marine heat wave in Cockburn Sound, southwest Australia.
1005 *Ocean Sci.*, 8(4), 545-550, doi:10.5194/os-8-545-2012, 2012.

1006 Rudnick, D. L.: Ocean research enabled by underwater gliders, *Ann. Rev. Mar. Sci.*, 8(1), 519-541,
1007 doi:10.1146/annurev-marine-122414-033913, 2016.

1008 Safonova, K., Meier, H. M., and Gröger, M.: Summer heatwaves on the Baltic Sea seabed contribute to oxygen
1009 deficiency in shallow areas, *Comm. Earth Environ.*, 5(1), 106, doi:10.1038/s43247-024-01268-z, 2024.

1010 Sampaio, E., Santos, C., Rosa, I. C., Ferreira, V., Pörtner, H.-O., Duarte, C. M., Levin, L. A., and Rosa, R.: Impacts
1011 of hypoxic events surpass those of future ocean warming and acidification, *Nat. Ecol. Evol.*, 5(3), 311-321,
1012 doi:10.1038/s41559-020-01370-3, 2021.

1013 Schaeffer, A., Roughan, M., & Wood, J. E.: Observed bottom boundary layer transport and uplift on the continental
1014 shelf adjacent to a western boundary current. *Journal of Geophysical Research: Oceans*, 119(8), 4922-4939,
1015 doi:10.1002/2013JC009735, 2014.

1016 Schaeffer, A., Roughan, M., Jones, E. M., and White, D.: Physical and biogeochemical spatial scales of variability in
1017 the East Australian Current separation from shelf glider measurements, *Biogeosciences*, 13, 1967–1975,
1018 doi:10.5194/bg-13-1967-2016, 2016a.

1019 Schaeffer, A., Roughan, M., Austin, T., Everett, J. D., Griffin, D., Hollings, B., ... and White, D.: Mean
1020 hydrography on the continental shelf from 26 repeat glider deployments along southeastern Australia, *Sci. Data*,
1021 3(1), 1-12, doi:10.1038/sdata.2016.70, 2016b.

1022 Schaeffer, A., and Roughan, M.: Subsurface intensification of marine heatwaves off southeastern Australia: The role
1023 of stratification and local winds, *Geophys. Res. Lett.*, 44(10), 5025-5033, doi:10.1002/2017GL073714, 2017.

1024 Schaeffer, A., Sen Gupta, A., and Roughan, M.: Seasonal stratification and complex local dynamics control the
1025 sub-surface structure of marine heatwaves in Eastern Australian coastal waters, *Commun. Earth Environ.*, 4(1),
1026 304, doi: 10.1038/s43247-023-00966-4, 2023.

1027 Schiller, A., Ridgway, K. R., Steinberg, C. R., and Oke, P. R.: Dynamics of three anomalous SST events in the Coral
1028 Sea, *Geophys. Res. Lett.*, 36(6), doi:10.1029/2008GL036997, 2009.

1029 Schroeder, T., Devlin, M. J., Brando, V. E., Dekker, A. G., Brodie, J. E., Clementson, L. A., & McKinna, L.:
1030 Inter-annual variability of wet season freshwater plume extent into the Great Barrier Reef lagoon based on
1031 satellite coastal ocean colour observations. *Marine Pollution Bulletin*, 65(4–9), 210–223,
1032 doi:10.1016/j.marpolbul.2012.02.022, 2012.

1033 Sen Gupta, A., Thomsen, M., Benthuisen, J. A., Hobday, A. J., Oliver, E., Alexander, L. V., ... and Smale, D. A.:
1034 Drivers and impacts of the most extreme marine heatwave events, *Sci. Rep.*, 10,
1035 doi:10.1038/S31598-020-75445-3, 2020.

1036 Siefert, R. L. and Plattner, G.-K.: The role of coastal zones in global biogeochemical cycles, *Eos Trans. AGU*,
1037 85(45), 470-470, doi:10.1029/2004EO450005, 2004.

1038 Skirving, W., Marsh, B., De La Cour, J., Liu, G., Harris, A., Maturi, E., ... and Eakin, C. M.: CoralTemp and the
1039 Coral Reef Watch coral bleaching heat stress product suite version 3.1, *Rem. Sens.*, 12(23), 3856,
1040 doi:10.3390/rs12233856, 2020.

1041 Smith, K. E., Burrows, M. T., Hobday, A. J., King, N. G., Moore, P. J., Sen Gupta, A., Moore, P. J., Thomsen, M.,
1042 Wernberg, T., and Smale, D. A.: Socioeconomic impacts of marine heatwaves: Global issues and opportunities,
1043 *Science*, 374, eabj3593, doi:10.1126/science.abj3593, 2021.

1044 Smith, K. E., Burrows, M. T., Hobday, A. J., King, N. G., Moore, P. J., Sen Gupta, A., Moore, P. J., Thomsen, M.,
1045 Wernberg, T., and Smale, D. A.: Biological impacts of marine heatwaves, *Ann. Rev. Mar. Sci.*, 15 (1), 119-145,
1046 doi:10.1146/annurev-marine-032122-121437, 2023.

1047 Stammer, D., Wunsch, C., & Ueyoshi, K.: Temporal changes in ocean eddy transports. *Journal of Physical*
1048 *Oceanography*, 36(3), 543-550, doi:10.1175/JPO2858.1, 2006.

1049 Tassone, S. J., Besterman, A. F., Buelo, C. D., Walter, J. A., and Pace, M. L.: Co-occurrence of aquatic heatwaves
1050 with atmospheric heatwaves, low dissolved oxygen, and low pH events in estuarine ecosystems, *Estuar. Coasts*,
1051 45(3), 707-720, doi:10.1007/s12237-021-01009-x, 2022.

1052 Testor, P., de Young, B., Rudnick, D. L., Glenn, S., Hayes, D., Lee, C. M., Pattiaratchi, C., Hill, K., Heslop, E.,
1053 Turpin, V., Alenius, P., ... and Wilson, D.: OceanGliders: a component of the integrated GOOS, *Front. Mar. Sci.*,
1054 6, 422, doi:10.3389/fmars.2019.00422, 2019.

1055 Walsh, S. J.: Commercial fishing practices on offshore juvenile flatfish nursery grounds on the Grand Banks of
1056 Newfoundland, *Netherlands J. Sea Res.*, 27(3-4), 423-432, doi:10.1016/0077-7579(91)90043-Z, 1991.

1057 Wang, Y., Holbrook, N. J., and Kajtar, J. B.: Predictability of marine heatwaves off Western Australia using a linear
1058 inverse model, *J. Clim.*, 36(18), 6177-6193, doi:10.1175/JCLI-D-22-0692.1, 2023.

1059 Weller, E., Holliday, D., Feng, M., Beckley, L., and Thompson, P.: A continental shelf scale examination of the
1060 Leeuwin Current off Western Australia during the austral autumn–winter, *Cont. Shelf Res.*, 31(17), 1858-1868,
1061 doi:10.1016/j.csr.2011.08.008, 2011.

1062 Wolanski, E. and Kingsford, M. (Eds.): *Oceanographic processes of coral reefs: Physical and biological links in the*
1063 *Great Barrier Reef (Second edition)*, CRC Press, Boca Raton, doi:10.1201/9781003320425, 2024.

1064 Woo, M. and Pattiaratchi, C.: Hydrography and water masses off the western Australian coast, *Deep Sea Research*
1065 *Part I: Oceanographic Research Papers*, 55(9), 1090-1104, doi:10.1016/j.dsr.2008.05.005, 2008.

1066 Woo, L. M. and Gourcuff, C.: Delayed Mode QA/QC Best Practice Manual Version 3.1 Integrated Marine
1067 Observing System, doi:10.26198/5c997b5fdc9bd, 2023.

1068 Wood, J. E., Schaeffer, A., Roughan, M., & Tate, P. M.: Seasonal variability in the continental shelf waters off
1069 southeastern Australia: Fact or fiction?. *Continental Shelf Research*, 112, 92-103, doi:10.1016/j.csr.2015.11.006,
1070 2016.

1071 Zhang, Y., Du, Y., Feng, M., & Hobday, A. J.: Vertical structures of marine heatwaves. *Nature Communications*,
1072 14(1), 6483, 2023.

1073 Zhao, Z., Holbrook, N. J. & Oliver, E. C. J.: An eddy pathway to marine heatwave predictability off eastern
1074 Tasmania. *Front. Clim.* 4: 907828, doi: 10.3389/fclim.2022.907828, 2022.

1075